THE ASTROPHYSICAL JOURNAL, 269:444–465, 1983 June 15

A MULTIFREQUENCY STUDY OF STAR FORMATION IN THE BLUE COMPACT DWARF GALAXY I Zw 36

F. VIALLEFOND
DEMIRM, Observatoire de Paris-Meudon, France; and Kapteyn Astronomical Institute, University of Groningen, The Netherlands

AND

TRINH X. THUAN[1,2,3]
Astronomy Department, University of Virginia; and Section d'Astrophysique, Centre d'Etudes Nucléaires de Saclay, France
Received 1982 August 11; accepted 1982 November 23

ABSTRACT

We present radio, near-infrared, optical, and ultraviolet observations of the blue compact dwarf galaxy (BCG) I Zw 36 ≡ Mrk 209 ≡ Haro 29. The H I distribution shows a core-halo structure. The core contains half of the mass and shows systematic motions. The halo is diffuse and contains several H I clumps. The visible star formation region is associated with the core but is slightly shifted with respect to the H I peak column density. The virial mass is 5 to 7 times the H I mass. I Zw 36 has about a tenth of the solar metallicity. Its dust-to-oxygen abundance ratio by mass is ~ 3 times greater than the ratio in the solar neighborhood. The near-infrared observations indicate the presence of an old stellar population of G and K giants.

Star formation models with an initial mass function of slope 1.5 (the Salpeter value is 1.35) and a burst age or duration of a few million years fit well the optical spectrophotometric measurements. To account for the metallicity, one previous burst of very short duration with a strength comparable to the present one is needed. Alternatively, no previous massive star formation is needed if there has been continuous star formation at a constant rate for the last 7 million years.

The old stellar population can account for the virial mass only if it is spatially much more extended than the young population. In that case, low-mass stars must have formed in the past independently from the burst producing the massive stars.

Very indirect evidence based on the dust content in I Zw 36 suggests that the column density of molecular hydrogen in I Zw 36 is 6 ± 3 times that of the neutral hydrogen, about the right amount to account for the virial mass. BCGs may be significantly more gas rich than previously believed.

Subject headings: galaxies: individual — galaxies: stellar content — radio sources: galaxies — radio sources: 21 cm radiation — stars: formation

I. INTRODUCTION

Since the pioneering work of Sargent and Searle (1970) which demonstrated the importance of studying the isolated dwarf emission-line galaxies, a large amount of observational material has been accumulated on these objects, which are also called isolated extragalactic H II regions. Two kinds of approaches have been used. The first one is statistical. A large number of these objects are observed with the same instrument by the same observer and are then used to study general trends in order to understand the physical parameters governing their evolution. The most recent studies in this direction are from Lequeux *et al.* (1979), French (1980), Kinman and Davidson (1981), and Kunth (1981) for optical spectroscopic observations, from Thuan and Martin (1981) for single-dish 21 cm observations, and from Thuan (1983) for near-infrared observations. The last two authors observed a large sample of blue compact dwarf ($M_B > -18$) galaxies (BCGs) selected from the lists of Haro, Markarian, and Zwicky.

The second approach consists in focusing on a single well chosen object and studying it in great detail, bringing together as much information in different spectral ranges as possible, in an attempt to build a realistic consistent physical picture for this object. We choose

[1]Visiting Astronomer, Kitt Peak National Observatory, which is operated by the Association of Universities for Research in Astronomy, Inc., under contract from the National Science Foundation.

[2]Guest observer with the *International Ultraviolet Explorer* satellite.

[3]Visiting Astronomer at the Infrared Telescope Facility which is operated by the University of Hawaii under contract from the National Aeronautics and Space Administration.

here the second approach. In this paper we report observations performed over six decades in frequencies, from the radio to the far-ultraviolet, on a single object I Zw 36 ≡ Mrk 209 ≡ Haro 29. We describe the radio observations in § II and the near-infrared observations in § III. In § IV, we present the spectrophotometric optical observations and discuss the metallicity of the galaxy. The ultraviolet observations are discussed in § V. In § VI, we combine all the observations in the different wavelength ranges together for a discussion on the dust content, the stellar content and the star formation history in I Zw 36. We summarize our conclusions in § VII.

II. RADIO OBSERVATIONS

a) *Object Selection*

While single-dish observations provide information on global properties such as hydrogen masses and velocity widths and have established that BCGs are very hydrogen-rich for their blue luminosity ($M_H/L_B \sim 0.4$), detailed interferometric H I studies of a few representative systems are needed to acquire information about the spatial distribution and the kinematics of the neutral hydrogen. Such information is essential for estimating the total masses of BCGs, quantities which are important for a better understanding of their evolution.

As of this writing there are only three BCGs with H I interferometric information. II Zw 40 was mapped by Gottesman and Weliachew (1972) with a spatial resolution of 5.6 kpc × 5.6 kpc and a velocity resolution of 21 km s^{-1}. II Zw 70 was mapped by Balkowski, Chamaraux, and Weliachew (1978) with a spatial resolution of 2.4 kpc × 4.2 kpc and a velocity resolution of 27 km s^{-1}. These relatively coarse maps showed that the H I size was much (> 5 times) larger than the optical size of the BCG, although in the case of II Zw 70 the interpretation was complicated by tidal interaction with a nearby companion, II Zw 71. Lequeux and Viallefond (1980) obtained a better velocity resolution (9.9 km s^{-1}) in their study of I Zw 18, but the spatial resolution (1.3 kpc × 1.6 kpc) remained insufficient. They could resolve the extended H I structure into six different clumps in velocity but not spatially. Moreover, they found that the total virial mass of I Zw 18 was ~ 10 times larger than the H I mass, a somewhat unexpected result since BCGs were believed to be relatively unevolved systems with most of their mass in neutral gas.

Clearly it was important to obtain an H I interferometric map of a BCG with better resolution to resolve the clumps spatially and to check if the large difference between the H I mass and the virial mass is a common property shared by BCGs. With the criteria of high spatial and velocity resolution in mind, we searched the list of BCGs of Thuan and Martin (1981) for a candidate with a large H I flux (to obtain a large signal-to-noise ratio), relatively nearby (to obtain spatial resolution), and favorably located in the sky for observing with the Westerbork Synthesis Radio Telescope (WSRT). A good candidate was I Zw 36, a galaxy described by Zwicky (1971) as a "blue compact coalesced with an irregular Sc galaxy," although careful examination of the Palomar Sky Survey prints reveals that the "Sc galaxy" can be more plausibly interpreted as a low-surface-brightness plume or jet coming from the blue compact galaxy. The observational characteristics of I Zw 36 are summarized in Table 1.

b) H I *Interferometric Observations*

The H I observations were obtained with the WSRT (Cassé and Müller 1974) in a 12 hour period using the digital cross-correlator. The parameters of the observa-

TABLE 1

OBSERVATIONAL CHARACTERISTICS OF I ZW 36

Parameter	Value
$\alpha(1950), \delta(1950)$[a]	$12^h23^m50^s.54, +48°46'12''.6$
l^{II}, b^{II}	134°.15, 68°.08
$a_{25} \times b_{25}$[b]	$52'' \times 46''$
m_B[c]	14.84
$(B-V)$[d]	0.51
$(U-B)$[d]	−0.51
$(V-R)$[d]	0.16
V_{Sys} (km s^{-1})[e]	280
ΔV_{50} (km s^{-1})[f]	47
M_B[g]	−14.5
D (Mpc)[h]	4.6
d (kpc)[i]	1.2
F_H ($10^6 M_\odot$ Mpc^{-2})	1.85 ± 0.02
M_H ($10^6 M_\odot$)	40.8 ± 0.6
L_B ($10^7 L_\odot$)[j]	9.9
M_H/L_B ($M_\odot/L_\odot$)	0.41

[a] Position of the optical core relative to 17 AGK3 reference stars measured on the Palomar Sky Survey prints. The accuracy is about 1".5 rms.

[b] The diameters quoted here include the low surface brightness plume. The blue compact core is considerably smaller, ~ 14".

[c] Observed apparent magnitude in the B system, inside a circular aperture of diameter a_{25} (Huchra 1977).

[d] The colors are corrected for galactic reddening and reduced to the diameter system a_{25} (Thuan and Martin 1981).

[e] Heliocentric systemic velocity.

[f] Velocity widths of the WSRT H I profile measured at 50% of the peak intensity and corrected for instrumental broadening.

[g] Absolute blue magnitude corrected for extinction as measured by the Balmer decrement.

[h] The distance was obtained by dividing the systemic velocity corrected to the Local Group velocity centroid (345 km s^{-1}) by the Hubble constant adopted to be $H_0 = 75$ km s^{-1} Mpc^{-1}.

[i] Linear major diameter.

[j] Calculated with $M_B(\text{Sun}) = 5.48$.

TABLE 2

WSRT PARAMETERS FOR THE RADIO OBSERVATIONS OF I ZW 36

Central frequency (MHz)	1419. 0945	4995.0
Approximate total bandwidth (MHz)	1.25	10.0
Date of observation	1979/11	1981/12
Number of 12-hour measurements	1	1
Total number of interferometers	18	40
Short spacing (m)	36	72
Largest spacing (m)	1260	2736
Spacing increment (m)	72	72
Radius of first grating ring $\alpha \times \delta$ (arcmin)	20.2×26.9	2.9×3.8
Half-power width of synthesized beam (arcsec)	27.9×37.2	3.7×5.0
Number of channels	31	1
Channel width (FWHM) and spacing (km s^{-1})	9.85, 8.3	
Range of heliocentric velocities (km s^{-1})	153.2, 400.9	
FWHM primary beam (arcmin)	37.6	12
Field center:		
α (1950)	$12^h23^m50^s.4$,	$12^h23^m51^s.0$
δ (1950)	48°47′24″,	48°46′13″
Observed sensitivity S_{rms} per channel (mJy/beam area)	3.1	0.25
T_b (K)/S (mJy/beam area)	0.6	2.8

tions are given in Table 2. The data were calibrated and Fourier-transformed according to the standard procedures. Data reduction and analysis were performed on the Groningen Interactive Image Processing System (GIPSY). Apart from I Zw 36 no other H I source was seen in the WSRT field at the level of sensitivity and in the range of velocities given in Table 2. The H I emission of I Zw 36 was detected in nine channels in the heliocentric velocity range from 252 to 318 km s^{-1}. Sixteen channels (channel centers from 153 to 219 km s^{-1} and from 327 to 376 km s^{-1}) were used to define a continuum map which was subtracted from the channel maps at velocities 228 to 327 km s^{-1} to produce continuum-free line maps. The resulting channel maps are shown in Figure 1. The noise on each of these maps is 3.1 mJy (rms) per synthesized beam. The total H I flux density in each line map was obtained by summing all the data values over an area sufficiently large to include all the H I emission from I Zw 36. The resulting values as a function of heliocentric radial velocity define a global H I profile (*heavy line* in Fig. 2) which, after Hanning smoothing to a velocity resolution of 16.6 km s^{-1}, can be compared with the single-dish profile obtained by Thuan and Martin (1981) with the NRAO[4] 300 foot (91 m) telescope (*light line* in Fig. 2). The integrated WSRT profile gives a total flux of 8.17 ± 0.12 Jy km s^{-1}. This value can be compared with the value of 9.7 ± 0.6 Jy km s^{-1} obtained by Thuan and Martin (1981). The slight discrepancy between these two values probably results from an incorrect determination of the baseline for the single dish spectrum causing an overestimate of the line emission in the low velocity side. If we integrate this 300 foot profile over the same range of velocities as in the case of the WSRT profile, we obtain 8.1 ± 0.6 Jy km s^{-1}, in excellent agreement with the present measurements; there is no extended H I emission which has not been seen by the Westerbork interferometer.

We construct velocity-position maps from the continuum-free channel maps (Fig. 1) and display them with GIPSY in order to inspect visually the places of significant H I emission in the data cube whose axes are right ascension α, declination δ, and heliocentric velocity v_H. Hanning smoothing was not applied to v_H in order to preserve the high velocity resolution. Since we are interested not only in the strongest features but also in features not far above the noise level, we need a criterion to decide on the reality of faint H I emission. In general, we consider such faint features to be significant only when they are extended in the data cube. For example, a faint H I feature at a level of 2 σ_{rms} per resolution element and which would be elongated in at least four consecutive channels in the (α, v_H)-plane would be considered real. For each position in the sky where it is decided that there is significant H I emission, the zeroth (total H I), first (velocity), and second (velocity dispersion) moments of the H I spectrum are computed. In order to eliminate as much as possible any subjectivity on the judgment of the reality of a faint H I features, the analysis of the spectra was performed three different times separated by several months intervals. The three sets of derived maps for the total H I, the velocity field, and the velocity dispersion field were then combined, making compromises in cases of discrepancies which were always found to be minor. The total H I

[4]The National Radio Astronomy Observatory is operated by Associated Universities, Inc., under contract with the National Science Foundation.

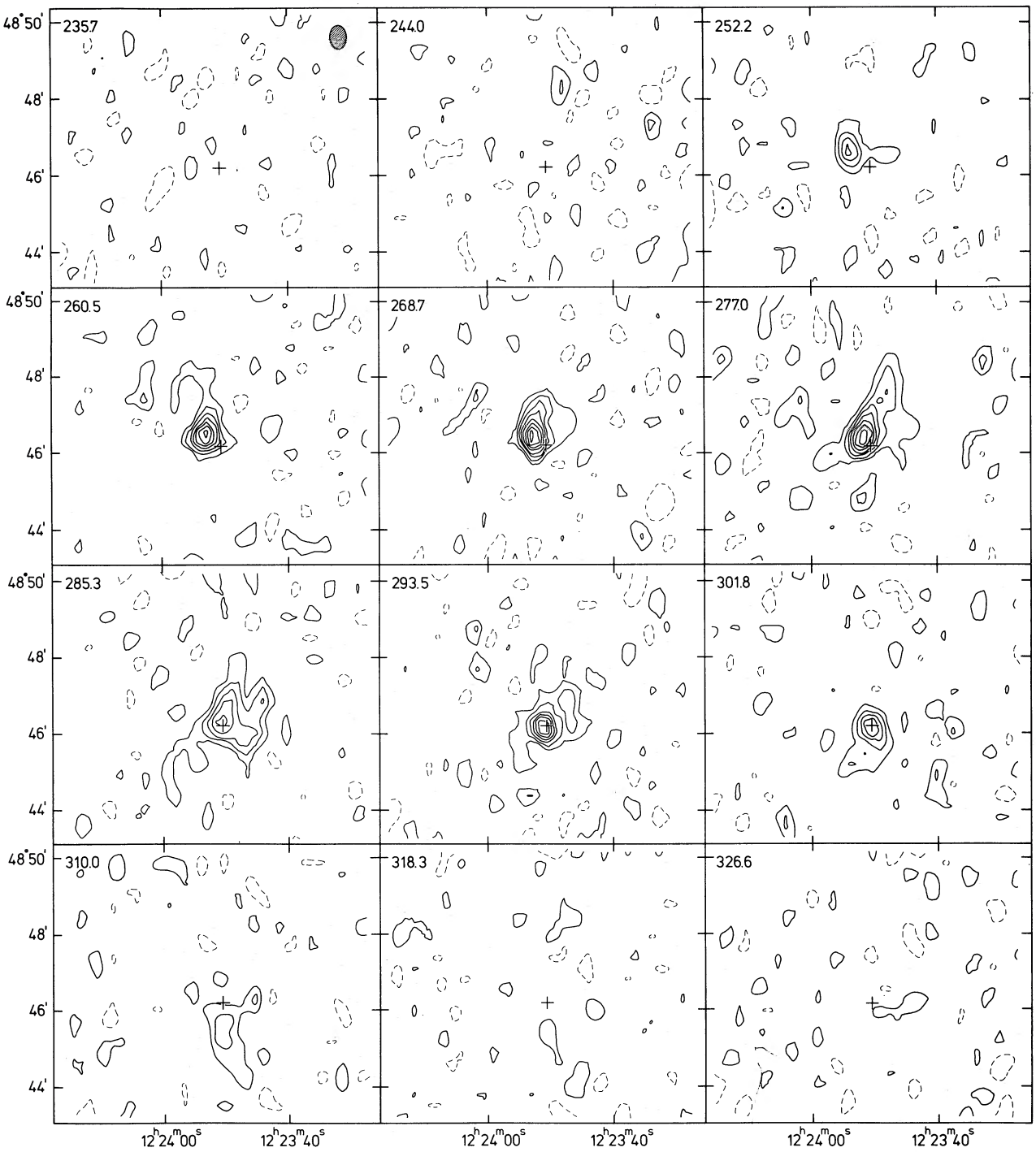

FIG. 1.—Channel maps of the 21 cm line radiation of I Zw 36. Isointensity contours at −2.7 K (*dashed*), 2.7 K, and multiples of 2.7 K (1.5 times the rms noise) are shown. The heliocentric radial velocity in km s^{-1} is given in the upper left corner of each map. The position of the brightest optical region is indicated by a cross in each map. The coordinates are for 1950.0.

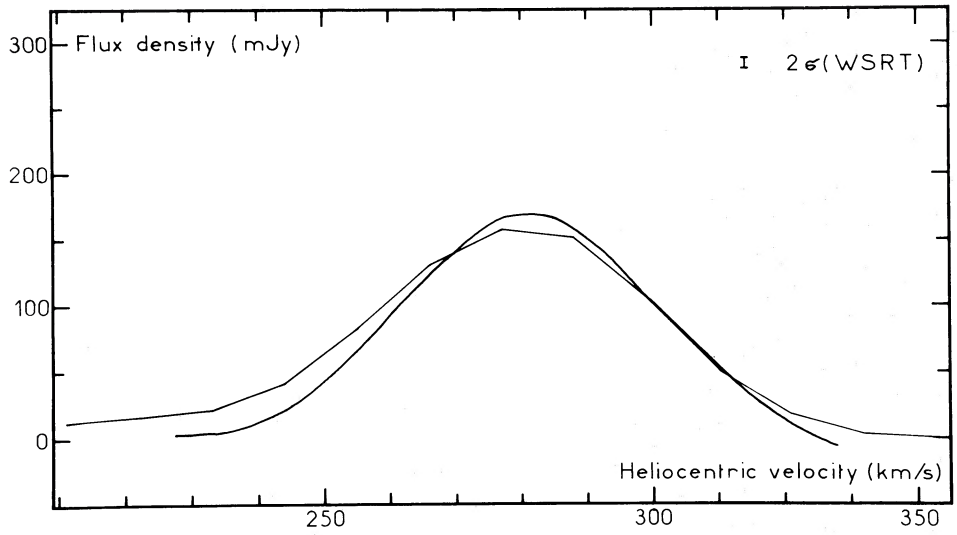

FIG. 2.—Global 21 cm spectrum of I Zw 36. The heavy line shows the present observations, Hanning-smoothed to a resolution of 11 km s^{-1}. The light broken line shows the profile obtained with the NRAO 300 foot (91 m) radiotelescope (Thuan and Martin 1981).

map is given in Figure 3 superposed on the Palomar Sky Survey blue image of I Zw 36.

It is evident from Figure 3 that the neutral gas in I Zw 36 shows a very clumpy structure. In fact, the spatial resolution is good enough to clearly show seven distinct H I cloud complexes. They are labeled in order of increasing right ascension, and their parameters are given in Table 3. Except for the main H I concentration (component 5), all components are unresolved by the beam. We discuss now each component in turn.

Component 1. This concentration is most visible in the channel maps (Fig. 1) at $v_H = 293.5$ km s^{-1}. It appears only 2.5 times above the rms noise level. Its reality is very uncertain; however, it has been considered because it is linked to the bulk of H I emission by some continuity in velocity.

Component 2. This concentration is most clearly visible on the channel maps at $v_H = 285.3$ km s^{-1}, but it can be seen up to $v_H = 310$ km s^{-1} where it appears as a point source at the 3.5 σ level. On the H I map it appears as a southwestern extension to the main H I concentration (component 5).

Component 3. This concentration has an asymmetric profile: it is most clearly visible at 277.0 km s^{-1}, but emission can be seen in several channels at higher velocities up to 318.3 km s^{-1} where it appears as the 1.5 σ level. It forms the northern extension of the main H I concentration.

Component 4. This concentration is visible at the 3 σ level in consecutive channels from 277.0 to 318.3 km s^{-1}. There is a gradient in velocity of 0.43 km s^{-1} $arcsec^{-1}$, with higher velocities on the western side.

Component 5. This is the main H I concentration which contains 54% of all neutral hydrogen in I Zw 36. It is likely to be associated with the region of active star formation due to the near coincidence of their positions. It is the only concentration resolved by the beam. Its deconvolved size and the position angle of its major axis are given in Table 3. The most ordered part of the velocity field of I Zw 36 (Fig. 4) is associated with this component. There is a maximum velocity gradient of 0.56 km s^{-1} $arcsec^{-1}$ along an axis which is not significantly different from the major axis of the H I distribution. This may be due to rotational motions. Because of beam-smearing, the true velocity gradient is very likely higher than the apparent one. The H I profiles along this axis (position angle 50°) are given in Figure 5.

The physical properties of component 5 can be estimated by considering two different models. First we consider the case where the gas is uniformly distributed with a density n(H I) in a sphere of radius r. After convolving the model with the Gaussian beamwidth at half-power (HPBW) of $28'' \times 37''$ in order to reproduce the observed full width at half-maximum (FWHM) geometric mean size, we obtain $r = 29''$, corresponding to 650 pc at a distance of 4.6 Mpc. The density is thus n(H I) = 0.77 cm^{-3}. The virial mass is 1.1×10^8 $M_\odot$, corresponding to a velocity dispersion of 11.9 km s^{-1}. However, the uniform model predicts a maximum H I column density which is too low compared to what is observed.

We next consider the more realistic case in which the gas density has a Gaussian distribution $n(\text{H I}) = n_0 \exp(-r^2/2a^2)$. In this case the maximum H I mean

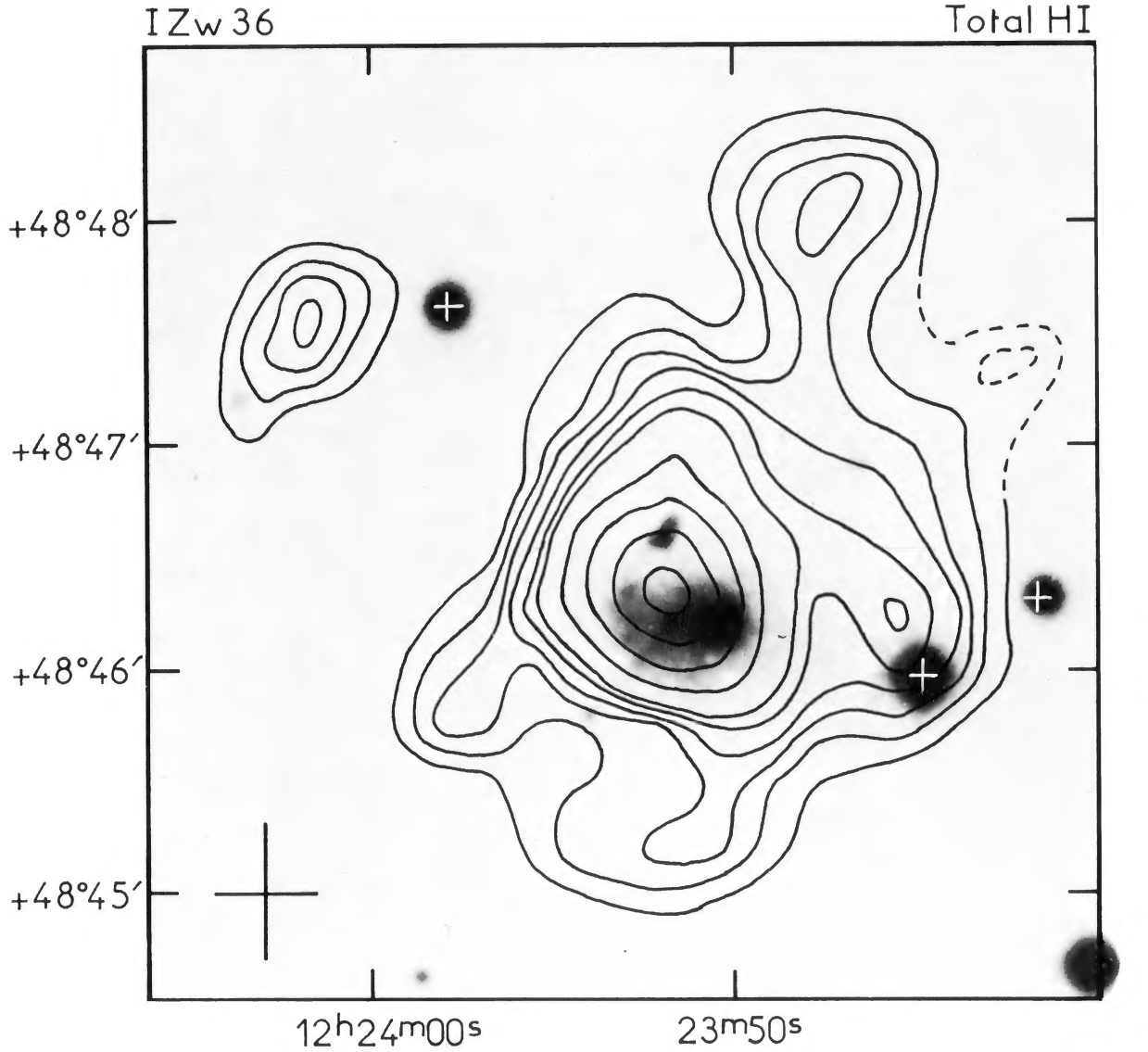

FIG. 3.—Map of the H I column density distribution of I Zw 36 superposed on a photograph reproduced from the blue print of the Palomar Sky Survey. The contours are from 41.1 to 369.8 K km s^{-1} in intervals of 41.1 K km s^{-1} and then from 369.8 to 739.5 K km s^{-1} in intervals of 123.3 K km s^{-1}. All features on this map have a signal-to-noise ratio $S/N \gtrsim 4$, except for the region with dashed contours where the S/N is only ~ 2.5. The cross indicates the beam size.

column density and the observed FWHM can be reproduced with $a = 450 \pm 70$ pc and $n_0 = 0.65 \pm 0.10$ cm^{-3}. The virial mass in this case is 1.5×10^8 $M_\odot$.

These estimates of the virial mass of component 5 are lower limits because systematic motions are neglected. They vary between 5 and 7 times the H I mass of 2.2×10^7 $M_\odot$. Most of the mass of this component is *not* in the form of atomic hydrogen.

Component 6. This component is a southeast extension of the main H I concentration, seen most clearly at the 3 σ level, in the channel map at 227.0 km s^{-1}. Its H I profile extends to higher velocities at the 1.5 σ level in three additional channels up to 302 km s^{-1}. Because of the extension in velocity, it is certainly real.

Component 7. At our level of detection, this component appears as an isolated clump in the northeast part of the H I map (Fig. 3). However, low-level H I emission escaping our detection and connecting this component to the other components cannot be ruled out. This component can also be seen as a separate component in the velocity field map (Fig. 4) and in the cut along the axis at position angle +50° (Fig. 5) where its H I profile is seen at 130″ from the origin. Component 7 is marginally elongated in the east-west direction with a possible

TABLE 3

PHYSICAL PARAMETERS OF THE H I COMPONENTS IN I Zw 36 (D = 4.6 Mpc)

Component	α (1950)	δ (1950)	V_H (km s^{-1})	ΔV_{50}	M(H I) ($10^6 M_\odot$)
1.....	$12^h23^m40^s.8$	48°47′21″	290	u	0.3±0.1
2.....	$12^h23^m45^s.6$	48°46′14″	299	28.1	1.3±0.3
3.....	$12^h23^m47^s.4$	48°48′02″	286	26.9	2.3±0.3
4.....	$12^h23^m51^s.2$	48°45′14″	295	38.6	1.0±0.3
5[a].....	$12^h23^m51^s.8$	48°46′20″	280	28.1	22.0±0.5
6.....	$12^h23^m57^s.2$	48°45′50″	290	32.4	1.3±0.3
7.....	$12^h24^m01^s.8$	48°47′32″	276	30.7	1.6±0.4
Halo	...	...	280	...	11.0±0.3
Total	$12^h23^m50^s.5$	48°46′28″	280	...	40.8±0.6

NOTE.—u = unresolved.

[a]Component 5 is the only resolved cloud. The geometric mean for the major and minor equivalent sizes is 39±3″. The deconvolution from the instrumental response gives an axial ratio of ~1.5 with a maximum extension along a direction at position angle ~50°.

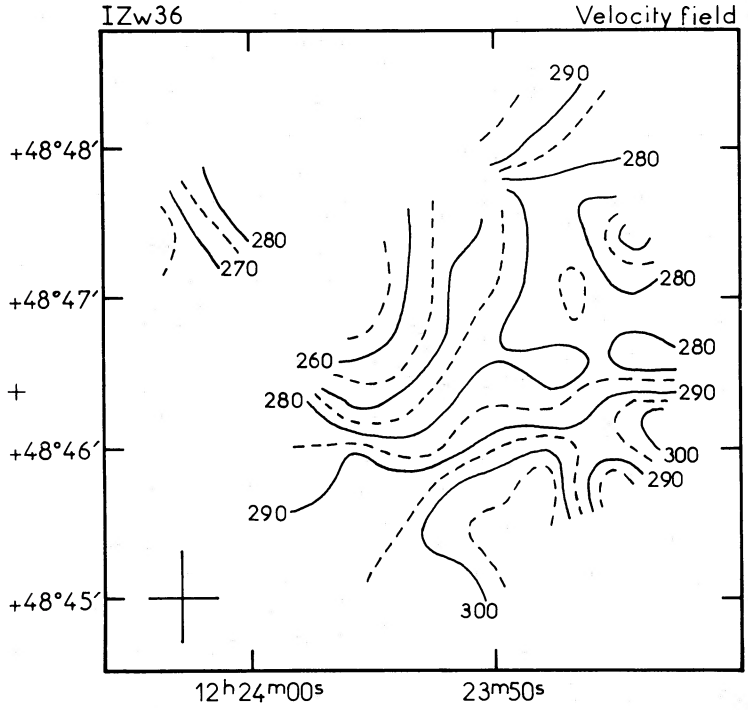

FIG. 4.—Velocity field. The contours, alternatively solid and dashed, are separated by an interval of 5 km s^{-1}. They are labeled by heliocentric velocities. The cross indicates the beam size.

velocity gradient of about 1 km s^{-1} arcsec^{-1} along this direction toward the West.

The total mass in H I in the seven complexes is 3×10^7 $M_\odot$. The total H I mass measured by the Westerbork telescope is 4.1×10^7 $M_\odot$, assuming the H I to be optically thin and at a distance of 4.6 Mpc. This suggests that there is a diffuse H I component of 1.1×10^7 $M_\odot$ which links all the complexes together.

The ratio of the virial mass M_V to the hydrogen mass M_H of I Zw 36 can be computed by using the cloud complexes just described as test particles to probe the gravitational field of the galaxy (Lequeux and Viallefond 1980). Using the equations given by Burbidge and Burbidge (1975), we obtain $M_V/M_H \sim 5$. It appears that about 80% of the total mass of the galaxy is not in the form of atomic hydrogen. We recall that we found a

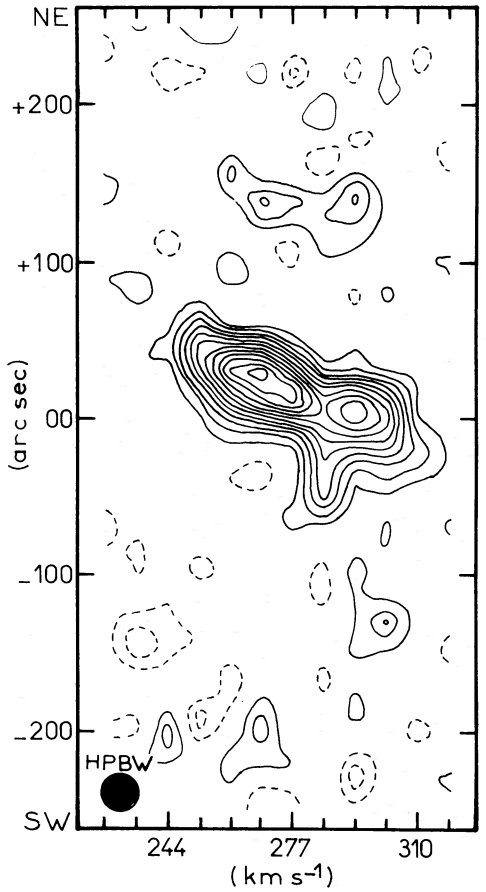

FIG. 5.—Position-velocity map of the 21 cm line radiation of I Zw 36 along an axis at position angle +50°. The origin for the positions is the optical position of the brightest part of the H II complex at $\alpha(1950) = 12^h23^m50^s.5$, $\delta(1950) = +48°46'13''$. Contours are −3.6, −1.8 (*dashed*), and 1.8 to 21.3 K (*solid*) by intervals of 1.8 K (the rms noise value). The size of one resolution element (HPBW) is given by the circular area.

similar result for the main H I concentration, with M_V/M_H varying between 5 and 7. We shall discuss the nature of the main constituent of the total mass of the galaxy in § VI.

c) *Comparison of the* H I *Properties of I Zw 36 with That of Other BCGs and* H I–H II *Associations in Late Type Galaxies*

I Zw 36 is the fourth BCG studied in the radio with an aperture synthesis instrument following the studies on II Zw 40, II Zw 70 and I Zw 18. Although the sample is still small, several important general observational properties for BCGs have emerged:

1. The H I distribution shows a core-halo structure. The core contains a significant fraction of the total H I mass, for example ~ 30% in I Zw 18 and ~ 50% in I Zw 36. The halo is diffuse and contains several much less massive H I clumps.

2. The visible star formation region is associated with the H I core. The size of the optical region is about one order of magnitude smaller than the H I size. The region of star formation is very near the neutral hydrogen peak surface density but does not coincide with it. There is a slight offset in all cases. With a Hubble constant of 75 km s^{-1} Mpc^{-1}, the offset is ~ 1.5 kpc in II Zw 40, ~ 1.8 kpc in II Zw 70, and ~ 0.5 kpc in both I Zw 18 and I Zw 36. This observational fact may be relevant for investigating possible mechanisms to trigger star formation in these systems.

3. In all cases, there is a velocity gradient associated with the densest H I region indicating the presence of systematic motions in these systems. At present the observations do not allow one to discriminate between rotation, expansion, or contraction (except maybe in the case of II Zw 70; see the discussion by Balkowski, Chamaraux, and Weliachew 1978).

4. The fractional neutral hydrogen gas mass M_H/M_V appears to be significantly less than unity in all cases. For II Zw 40, $M_H/M_V \lesssim 0.5$; for both I Zw 18 and I Zw 36, M_H/M_V is of the order of 0.1–0.2, and for II Zw 70 $M_H/M_V \approx 0.2$. Clearly a substantial fraction of the total mass of a BCG is in a form other than atomic hydrogen.

It is also interesting to compare the H I properties of I Zw 36 with that of the giant H I–H II complexes seen in spiral galaxies such as M101 and discussed by Viallefond, Goss, and Allen (1982). The BCG is observationally indistinguishable from the outer H I–H II associations in M101, such as NGC 5471. They both have high electronic densities ($n_e \sim 10$ cm^{-3}) and low mean H I densities [n(H I) ~ 0.5 cm^{-3}] as compared to the H I–H II associations in the inner parts of spiral galaxies.

d) *Radio Continuum Emission*

We have examined the channels free of line emission for possible continuum emission at 1.4 GHz. After averaging these channels, an unresolved continuum source was seen above the noise at the 4 σ level at the position $\alpha(1950) = 12^h23^m52^s.5$ and $\delta(1950) = +48°46'01''$, with a flux density of 3.4±0.7 mJy. Although the signal-to-noise ratio is low, we are confident that the detection is real because the continuum source appears in both sets of continuum channels on either side of the H I line and disappears if one set is subtracted from the other.

We have also observed I Zw 36 at Westerbork in the continuum at 5 GHz to obtain spectral information. The WSRT parameters are summarized in Table 2, and the map is shown in Figure 6.

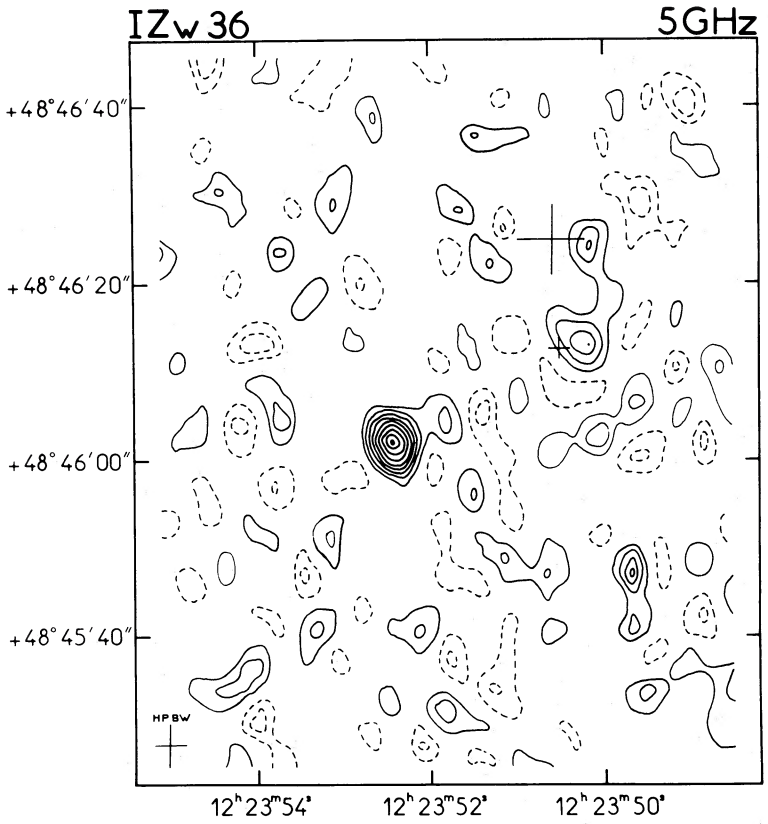

FIG. 6.—Map of the continuum emission at 5 GHz. Contour levels are −0.18, −0.09 (*dashed*), +0.09 to 0.79 K (*solid*) by intervals of 0.09 K (the rms noise value). Coordinates are 1950.0. The small cross indicates the optical position given in Table 1. The large cross indicates the position where the near-infrared observations were obtained, with the size of the cross representing the aperture size.

Two sources associated with I Zw 36 are seen.[5] Source 1 is the brightest source and the only one exceeding 2 mJy at 5 GHz in the 7'.0 × 9'.2 field. Its position is in excellent agreement with that of the 1.4 GHz continuum source, and its flux is 3.4 ± 0.03 mJy. Hence this source has a flat radio spectrum between 1.4 and 5 GHz and is very likely of thermal nature. It is extended (2".2 deconvolved FWHM) and lies at the southeast edge of the optical complex with which it is undoubtedly associated (Fig. 3). The probability that there is a thermal and extended background source at 20" from the optical centroid of I Zw 36 is extremely small. The fact that there is no bright H II region at the location of source 1 may mean that there is a significant amount of visual extinction at that position (§ VI).

Source 2 is much weaker and is detected only at the 4 σ level. It is marginally extended (1".60 ± 0".15 deconvolved FWHM). We believe in its reality because of the coincidence of its position with that of the brightest optical knot in I Zw 36. The latter is given in Table 1 and was measured on the Palomar Sky Survey with an accuracy of ~ 1".5. The flux density of this source at 5 GHz is 1.25 ± 0.24 mJy. It was not seen at 1.4 GHz, but using a 3 σ upper limit its spectral index between 1.4 and 5 GHz has to be greater than −0.3. It is most likely that the radio flux is of thermal nature and is produced by free-free emission from the star formation region responsible for the optical line emission described in § IV.

From these observations, we can derive useful physical parameters for the two radio continuum sources. These are listed in Table 4. They have been derived using standard equations for extragalactic H II complexes (Viallefond 1983) modeled as cylinders aligned along the line of sight and with their lengths equal to their diameters. The electron temperature was taken to be 14,500 K (§ IV).

III. NEAR-INFRARED OBSERVATIONS

As shown by Struck-Marcell and Tinsley (1978), infrared colors are in principle much more sensitive to the

[5]We have detected one additional background point source at the position $\alpha(1950) = 12^h24^m21^s.53$ and $\delta(1950) = 48°48'04".7$ with a flux density of 8.1 mJy at 5 GHz and a spectral index of −1.4 between 1.4 and 5 GHz.

TABLE 4

PHYSICAL PARAMETERS OF THE TWO RADIO CONTINUUM SOURCES

Parameter	Source 1	Source 2
U (pc cm^{-2})	609 ±14	440 ±30
$N_{\rm Lyc}$ (10^{51} phot s^{-1})	5.3 ± 0.4	1.9 ± 0.4
$d_{\rm H\,II}$ (pc).....	94 ±18	59 ± 5
n_e (cm^{-3}).....	41 ±10	47 ± 2
EM (10^5 pc cm^{-6})	1.50± 0.45	1.3 ± 0.5
$M_{\rm H\,II}$ (10^6 $M_\odot$)	0.62± 0.20	0.19± 0.04

presence or absence of underlying old stars than *UBV* colors. We thus observed I Zw 36 in the *JHK* bands in order to check for the possible presence of an old stellar population and see whether it can account for the large total mass revealed by the H I interferometric observations (§ II).

The observations were made with the NASA 3 m Infrared Telescope Facility (IRTF) on Mauna Kea during the night of 1982 March 30. The IRTF InSb photometer was used with a 7″.8 aperture and a beam throw of 2′ north-south. Since we wanted to avoid contamination to the infrared measurement by the possible presence of young supergiant stars in the active star-forming region, we observed at the position of the H I centroid, at $\alpha(1950) = 12^{\rm h}23^{\rm m}50\overset{\rm s}{.}6$ and $\delta(1950) = 48°46'25''$. The region observed avoids the brightest part of the galaxy and is 12″.4 north of the optical centroid given in Table 1. These observations are part of a more extensive program undertaken by one of us (Thuan 1983), and the magnitude to flux calibration based on α Lyrae will be described elsewhere. The observed magnitudes and flux densities are given in Table 5.

Also given are the flux densities corrected for galactic extinction and extinction in I Zw 36. The galactic extinction was calculated using the observed galactic H I column density in the direction of I Zw 36 (Heiles 1975) and the galactic extinction curve of Savage and Mathis (1979). The extinction in I Zw 36 was estimated using the H I column density in the BCG at the observed position, assuming that $N_{\rm H}/E(B-V)$ is proportional to the abundance of dust (§ VI*a*) and the source is halfway along the line of sight in the H I cloud. The extinction corrections are in all cases very small.

We now discuss the nature of the near-infrared radiation. Three possible sources can be thought of which can account for the observed fluxes: dust, emission from transitions in the ionized gas, and stars in the form of dwarfs, giants, or supergiants. The dust hypothesis can be ruled out because the flux density decreases steadily from 1.25 to 2.2 μm. We next calculate the contributions to the J, H, K bands from the ionized gas. At the observed position, using the map shown in Figure 6, we obtain an upper limit (2 σ) of 0.2 K for the observed brightness temperature at 5 GHz. The upper limits for the free-free and free-bound radiation in the three bands are then about 0.03 mJy at the three wavelengths for the region covered by the 7″.8 aperture. The emission from the two-photon decay of the $2\,^2S$ level of H I is negligible, being one order of magnitude smaller. The final *JHK* fluxes corrected for extinction and emission from the ionized gas are given in the last column of Table 5. These fluxes are of stellar origin. We shall discuss the nature of the stars and whether they can account for the virial mass of I Zw 36 in § VI.

IV. SPECTROPHOTOMETRIC OPTICAL OBSERVATIONS AND CHEMICAL COMPOSITION

The observations were obtained in 1981 April at Kitt Peak National Observatory (KPNO) with the 2.1 m telescope and the Image Intensifier Dissector Scanner (IIDS) used in conjunction with the gold image tube spectrograph. Integration times of 1000 s were used with a circular 6″.1 diameter entrance aperture. Two gratings were used covering the wavelength range 3400–5200 Å in the blue and 5600–7400 Å in the red. The half-width resolution was 6.7 Å for both settings. The aperture was centered on the brightest optical part of the galaxy. The raw spectra were sky-subtracted, calibrated, and reduced using standard KPNO routines. The calibration was derived from standard star fluxes by Stone (1974) and Oke (1974). The resulting energy distributions are given in Figures 7 and 8. The observed

TABLE 5

NEAR-INFRARED OBSERVATIONS

λ (μm)	m (mag)	Flux Densities (mJy) Observed	Corrected for Galactic Extinction	Corrected for Extinction in I Zw 36	Corrected for Ionized Gas Emission
1.25 (J)	15.59±0.05	0.94±0.05	0.97±0.05	1.01±0.05	0.98±0.05
1.65 (H) ...	15.19±0.06	0.85±0.05	0.87±0.05	0.89±0.05	0.86±0.05
2.20 (K) ...	15.09±0.11	0.59±0.06	0.60±0.06	0.61±0.05	0.58±0.05

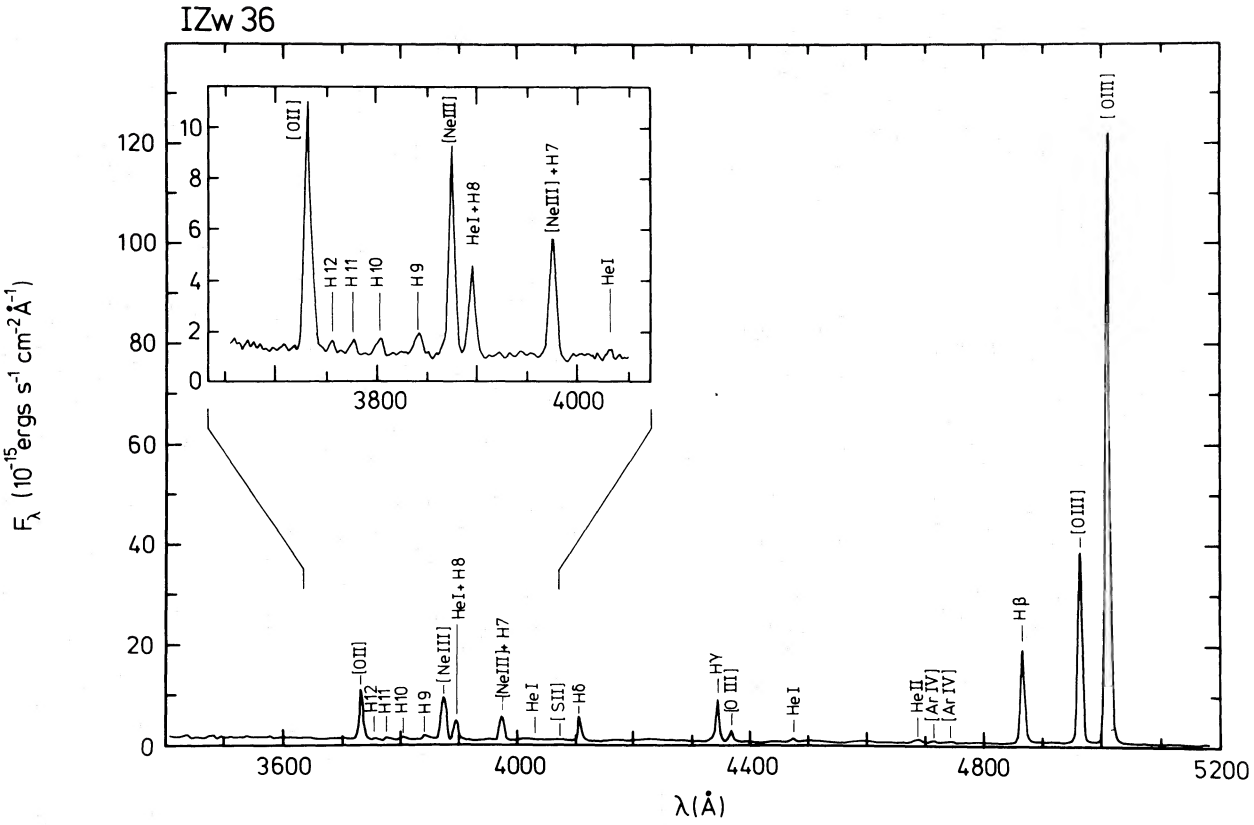

FIG. 7.—Blue IDS optical spectrum of I Zw 36 with a resolution (FWHM) of 6.7 Å

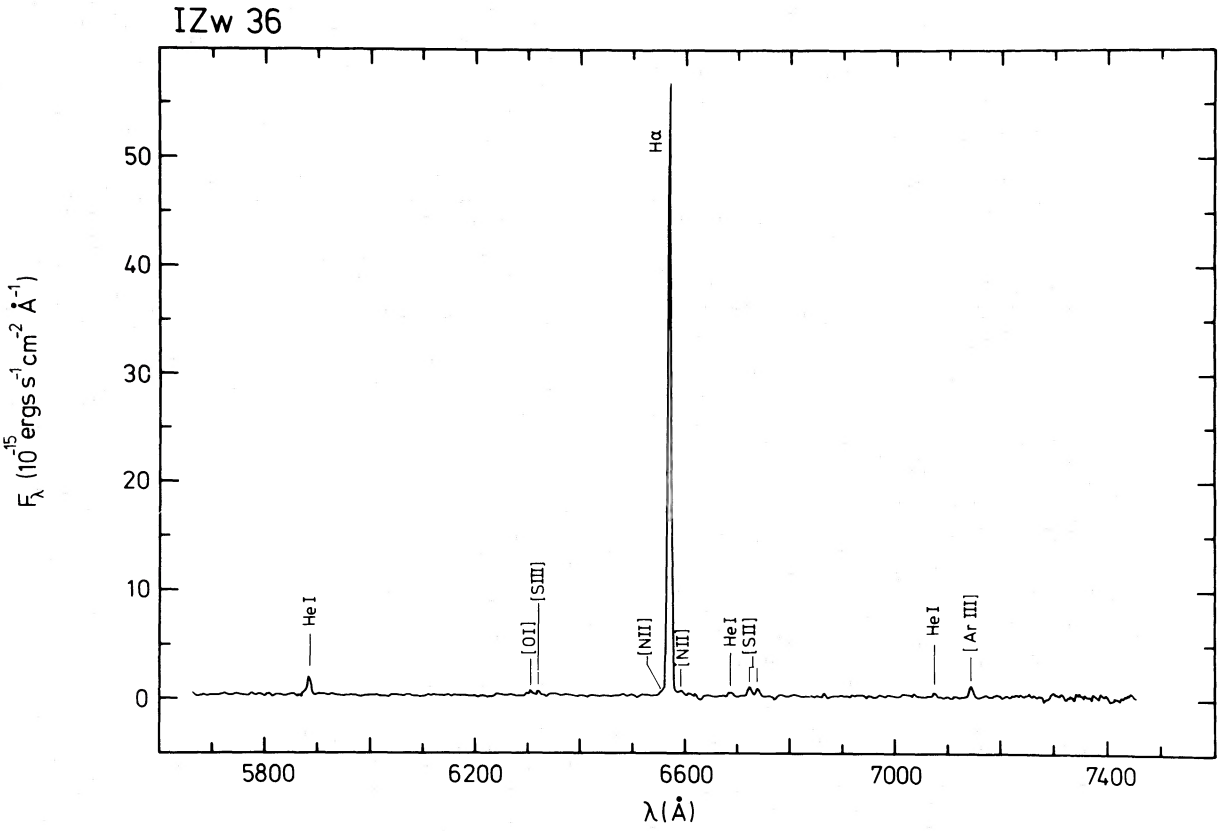

FIG. 8.—Red IDS optical spectrum of I Zw 36 with a resolution (FWHM) of 6.7 Å

(F) and dereddened (I) line fluxes in ergs cm^{-2} s^{-1} are given in Table 6. The reddening correction has been computed by fitting the apparent $H\beta/H\gamma/H\delta$ intensity ratios, assuming that these are pure recombination lines, to the ones computed by Brocklehurst (1971) for $T_e =$ 15,000 K and $n_e = 100$ cm^{-3}. The galactic extinction law (Whitford 1958) has been used. This is justified by the fact that the ratio $E(\lambda 4340-\lambda 4861)/E(\lambda 4101-\lambda 4861) = 0.62 \pm 0.10$ for I Zw 36 is in good agreement with the value of 0.70 for the average galactic extinction curve. The color excesses $E(\lambda_i - \lambda_j)$ have been derived by comparing the ratio of two Balmer lines at wavelengths λ_i and λ_j with the theoretical ratio assuming pure recombination lines (case B). We obtain $E(\lambda 4340 - \lambda 4861) = 0.15 \pm 0.06$ and $E(\lambda 4101 - \lambda 4861) = 0.24 \pm 0.07$. Absorption in the stellar continuum, which would reduce the apparent Balmer emission intensities, is unimportant in the case of I Zw 36. The equivalent widths of the $H\beta$, $H\gamma$, and $H\delta$ absorption lines in early type stars have equivalent widths of the order of 3 or 4 Å, considerably smaller than the emission equivalent widths. Small pointing and guiding errors and seeing variations will cause the absolute fluxes in the red not to match those in the blue. Consequently all the line intensities in the 5600–7400 Å range were multiplied by a constant factor equal to 1.4. This gray shift was determined by adjusting the observed $H\alpha/H\beta$ ratio to the theoretical one (Brocklehurst 1971). The resulting accuracy of the blue to red line intensity ratios for bright lines can be estimated by comparing the theoretical and observed He I (4472/5876) line intensity ratios, and the error is probably less than 50%. Con-

TABLE 6

OPTICAL LINE FLUXES

Line	F_λ Observed	I_λ Dereddened	Error Code[a]
3727 [O II]	51.4	70.1	a
3750 H12	1.3	1.8	b
3770 H11	1.5	2.0	b
3797 H10	2.5	3.3	b
3835 H9	3.8	5.0	b
3869 [Ne III]	38.0	49.5	a
3889 He I + H8	15.9	20.5	a
3967 + 3970 [Ne III] + Hε	22.9	29.0	a
4026 He I	0.7	0.8	d
4068 + 4076 [SII]	0.6	0.7	d
4101 Hδ	21.0	25.8	a
4340 Hγ	41.3	47.5	a
4363 [O III]	10.3	11.8	a
4471 He I	2.0	2.2	a
4686 He II	4.1	4.3	b
4715 [Ar IV]	1.3	1.3	d
4746 [Ar IV]	0.9	0.9	d
4861 Hβ	100.0	100.0	a
4922 He I	1.9	1.9	b
4959 [O III]	203.7	198.1	a
5007 [O III]	651.6	624.6	a
5876 He I	12.7	10.4	a
6300 [O I]	5.0	3.8	c
6312 [S III]	2.3	1.7	c
6548 [N II]	2.9	2.1	b
6563 Hα	388.2	279.4	a
6583 [N II]	4.9	3.5	b
6678 He I	2.2	1.6	b
6716 [S II]	5.9	4.2	a
6730 [S II]	4.3	3.1	a
7076 He I	2.1	1.4	d
7136 [Ar III]	6.7	4.5	d

$W_\lambda(H\beta) = 238 \pm 23$ Å

$F(H\beta)$ (observed) $= (1.615 \pm 0.036) \times 10^{-13}$ ergs cm^{-2} s^{-1}

$C(H\beta) = 0.41 \pm 0.12$[b]

[a] Error estimates: a: $\lesssim 10\%$; b: $\lesssim \pm 20\%$; c: $\lesssim \pm 30\%$; d: $\lesssim \pm 40\%$.

[b] $C(H\beta)$ is defined as: $\log [I(\lambda)/I(H\beta)] = \log [F(\lambda)/F(H\beta)] + F(\lambda)C(H\beta)$, where $F(\lambda)$ is the Whitford 1958 reddening function normalized at $H\beta$.

servative estimates of the statistical uncertainties in the line intensities are also given in Table 6.

We derive now the physical conditions and the metallicity in the visible region of I Zw 36. The atomic parameters used are the same as those used by Kunth (1981). The [O III] lines imply $T_e = 14{,}500 \pm 500$ K. The [S II] doublet ratio gives a mean electron density for the [S II] zone $n_e(\text{S II}) = 135 \pm 50$ cm^{-3}. We derive elemental abundances by standard procedures, neglecting temperature fluctuations (a reasonable assumption for low-density H II regions) and using the ionization correction factors given in Lequeux *et al.* (1979). The ionic abundances and final abundance ratios are given in Tables 7 and 8. The $N(\text{He}^+)/N(\text{H}^+)$ abundance ratio was derived from the 4471, 5876, and 6678 to Hβ ratios with relative weights of 1, 2, and 1, respectively, because of their relative intensities. The He abundance is the sum of $N(\text{He}^+)$ and $N(\text{He}^{++})$, both observed directly. The heavy-element abundance, Z, was obtained by assuming that it is proportional to the oxygen abundance and that O constitutes 45% of Z by mass. The Y and Z values for I Zw 36 are given in Table 8. Like all other known BCGs, I Zw 36 is metal deficient: it has a metallicity of about one-seventh the metallicity of Orion. With an H II mass in the star formation region of $1.9 \pm 0.4 \times 10^5$ $M_\odot$ (Table 4), the oxygen mass associated with the H II region is 16 ± 3 $M_\odot$. If this metallicity is characteristic of the entire H I component 5 (§ II*b*) with which the star formation region is associated, the total oxygen mass would be 1900 ± 300 $M_\odot$.

V. FAR-ULTRAVIOLET OBSERVATIONS

Finally we discuss the far-ultraviolet spectrum of I Zw 36 obtained with the *International Ultraviolet Explorer* (*IUE*) satellite. The spectrum shown in Figure 9 was obtained in 1980 December using the low resolution mode, the short wavelength camera (1150–1950 Å), and the large entrance aperture (10″ × 20″). The integration time was 407 minutes. The far-UV spectrum has a continuum which increases steadily from 1950 Å to 1150 Å. It does not show the characteristic P Cygni profiles of prominent absorption lines such as Si IV λ1403 and C IV λ1550 often seen in UV spectra of BCGs (Thuan, Fanelli, and O'Connell 1983) and some H II regions in nearby galaxies like NGC 604 (Rosa 1980).

Contrary to the optical spectrum (Figs. 7 and 8) where many nebular emission lines are observed, the C III] λ1909 is the only certain nebular line in the far-UV spectrum. This is because the stellar continuum is much more important in the UV than in the optical with respect to the nebular emission. The strength of the collisionally excited nebular line C III] λ1909 is sensitive to both the metallicity and the effective temperature T_{eff} of the ionizing stars. The C III] λ1909 line is easily detected in low-metallicity and high-excitation (high [O III]/Hβ ratio) galaxies such as I Zw 36, the H II regions in the Magellanic Clouds (Dufour, Shields, and Talbot 1982), or H II complexes such as NGC 5471 (Rosa 1980) in M101 and NGC 2363 (*IUE* archives) in NGC 2366, but it is not observed in H II complexes

TABLE 7

IONIC ABUNDANCES[a] IN I ZW 36

[He$^+$]	[He^{++}]	[N$^+$]	[O$^+$]	[O^{++}]	[Ne^{++}]	[S$^+$]	[S^{++}]
10.79 ± 0.15	9.58 ± 0.09	5.53 ± 0.10	6.84 ± 0.11	7.86 ± 0.08	7.13 ± 0.11	4.86 ± 0.11	5.87 ± 0.21

NOTE.—The uncertainties do not include systematic errors in the reddening corrections and the red-blue matching. These are estimated to be smaller than 0.10 in the log.

[a] $[\text{X}^i] = 12 + \log [N(\text{X}^i)/N(\text{H}^+)]$.

TABLE 8

LOGARITHMIC ABUNDANCE RATIOS[a]

	O	N/O	S/O	Ne/O	Y	Z
I Zw 36	7.93 ± 0.07	-1.31	-1.98	-0.73	0.215 ± 0.020	0.0013 ± 0.0001
I Zw 36/Orion[b] ...	-0.83 ± 0.16	-0.32	-0.43	$+0.12$	...	...
I Zw 36/Sun[b].....	-0.98	-0.38	-0.29	$+0.07$	...	...

[a] $[\text{O}] = 12 + \log [N(\text{O})/N(\text{H})]$, $\text{X/O} = \log [N(\text{X})/N(\text{O})]$, Y and Z are abundances by mass. The accuracy of the logarithmic abundance ratios is estimated to be better than 0.2 in the log except for S/O because S III, the dominant species, is not observed here.

[b] The abundances for Orion and the Sun are from Lequeux *et al.* 1979.

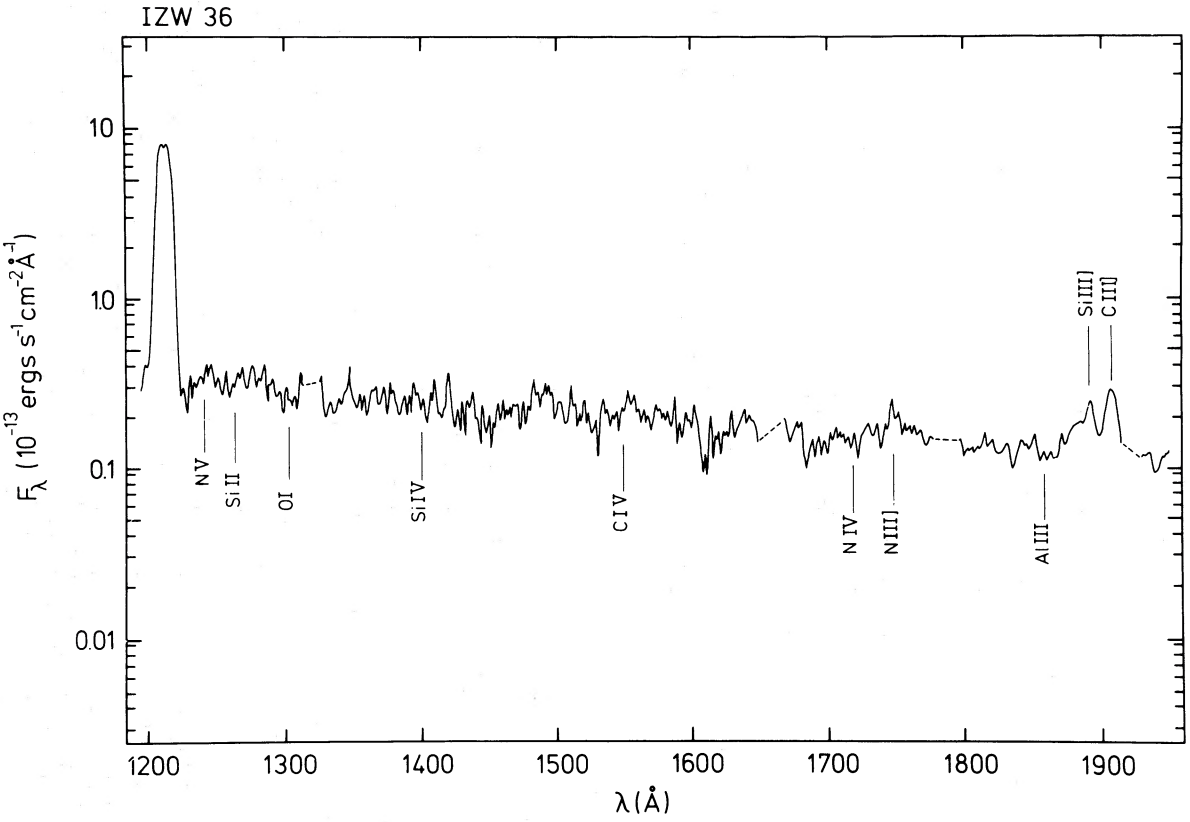

FIG. 9.—*IUE* UV spectrum of I Zw 36 with a resolution of about 7 Å

such as NGC 604 (Rosa 1980) in M33 or NGC 5461 (*IUE* archives) in M101 which have higher metallicity and lower excitation.

We use the C III] λ1909 line to determine the internal extinction A_{1909}. The procedure is the following: first, determine the ratio $(F_{1909})_c/I_\beta$ where $(F_{1909})c$ is the observed line flux corrected for extinction from the Galaxy and I_β is the intrinsic Hβ flux derived from the 5 GHz radio flux S (5 GHz); then, compare with the theoretical I_{1909}/I_β with the appropriate values of O/H and $T_{\rm eff}$ in Stasinska's (1982) models to derive A_{1909}. The results are given in Table 9, where, in addition to I Zw 36, we have also considered three other H II complexes where the λ1909 line has been detected for comparison.

The Galactic extinction has been calculated using $A_{1900}/E(B-V)=8.0$ and $N(\text{H I})/E(B-V)=5.8\times 10^{21}$ H atoms cm^{-2} mag^{-1} (Savage and Mathis 1979). The H I column density N(H I) is taken from the Berkeley H I survey (Heiles 1975). The intrinsic Hβ fluxes are computed from the radio fluxes with the temperatures T(O III) listed in Table 9. Stasinska's (1982) models assume a solar C/O ratio. If carbon is depleted relative to oxygen in metal-poor galaxies compared to the solar neighborhood (Dufour, Shields, and Talbot 1982), the A_{1909} listed in Table 9 are upper limits. Table 9 also gives the ratios of A_{1909} to the optical color excesses which characterize the extinction curves of the galaxies under discussion. These ratios can be compared with the corresponding ratios for the Galaxy which are $A_{1909}/E(\alpha-\beta)=-6.67$, $A_{1909}/E(\gamma-\beta)=17.8$, and $A_{1909}/E(\delta-\beta)=13.3$.

It can be shown that the corrections for extinction of the C III] λ1909 nebular line and of the light from the ionizing star cluster are about the same, independent of their relative spatial distribution. The dereddened spectrum is then given by

$$\frac{I_\lambda}{I_{1900}}=\left(\frac{F_\lambda}{F_{1900}}\right)_c \text{dex}\, C_{1900}\frac{E(\lambda-1900)}{A_{1900}},$$

where $C_{1900}\approx C_{1909}=0.40\ A_{1909}$, $E(\lambda-1900)/A_{1900}$ is the ratio of the selective to total extinction as given by the extinction law in the object, and $(F_\lambda/F_{1900})_c$ is the normalized flux corrected for extinction in the Galaxy. To correct for Galactic extinction, the law given by Savage and Mathis (1979) is used with $E(B-V)$ determined from N(H I) in the direction of I Zw 36 (Heiles 1975).

TABLE 9

UV EXTINCTION DETERMINATION FROM THE C III] λ1909 LINE IN EXTRAGALACTIC H II COMPLEXES

Parameter	I Zw 36	NGC 5471[a]	NGC 5455[b]	NGC 2363[c]
F_{1909} (10^{-13} ergs s^{-1} cm^{-2}) ...	1.64±0.20	1.53±0.20	0.54±0.18	4.53±0.17
A_{1909} (Gal)[d] (mag)	0.24±0.04	0.13±0.04	0.13±0.04	0.71±0.04
T(O III) (10^4 K)	1.45	1.24	1.62	1.56
$S_{5\ GHz}$ (mJy)	1.24±0.25	12±3	5.5±2	9.6±0.7
I_β (10^{-13} ergs s^{-1} cm^{-2}).....	3.65±0.73	38.3±9.6	19.4±7.1	27.2±2.0
$(F_{1909})_c/I_\beta$	0.56±0.20	0.05±0.02	0.03±0.02	0.32±0.05
O/H (10^{-4})	0.85	1.55	3.4	0.79
T_{eff} (10^4 K)	4.2 to 5.0	4.0 to 4.6	~3.9	~4.8
I_{1909}/I_β	2.1	2.2	0.54	2.1
A_{1909} (obj)[e] (mag)	1.44±0.56	4.22±1.74	3.10±2.40	2.04±0.33
$A_{1909}/E(\alpha-\beta)_{obj}$	[f]	−12.6	−11.9	−10.7
$A_{1909}/E(\gamma-\beta)_{obj}$	11.5	29.7	15.5	680
$A_{1909}/E(\delta-\beta)_{obj}$	6.9	20.6	9.4	227

[a]Radio data from Israel, Goss, and Allen 1975; optical data from Rayo, Peimbert, and Torres-Peimbert 1982; UV data from Rosa 1980.

[b]Radio data from Israel, Goss, and Allen 1975; optical data from Shields and Searle 1978; UV data from *IUE* archives.

[c]Radio data from Viallefond 1983; optical data from Kennicutt, Balick, and Heckman 1980; UV data from *IUE* archives.

[d]Galactic extinction.

[e]Extinction in the object.

[f]$E(\alpha-\beta)$ not determined because the Hα and Hβ lines are not observed simultaneously (§ IV).

TABLE 10

FAR-UV CONTINUUM FLUX DENSITIES IN I ZW 36

λ (Å)	F_λ/F_{1900} Observed	$(F_\lambda/F_{1900})_c$	I_λ/I_{1900} Gal	I_λ/I_{1900} LMC	I_λ/I_{1900} SMC
1900	1.00	1.00	1.00	1.00	1.00
1600	1.54	1.54	1.57	1.64	1.57
1390	1.98	2.01	2.18	2.65	2.73
1250	2.80	2.91	3.68	5.00	4.95

NOTE.—$(F_{1900})_{obs} = 1.1 \times 10^{-14}$ ergs cm^{-2} s^{-1} Å^{-1}. $C_{1900} = 0.67 \pm 0.22$. $(F_\lambda/F_{1900})_c$: corrected for Galactic extinction.

We have considered three different extinction laws to correct I Zw 36 for internal extinction: the extinction curve for the Galaxy (Savage and Mathis 1979), that for the Large Magellanic Cloud (Nandy *et al.* 1980), and that for the Small Magellanic Cloud (Rocca-Volmerange *et al.* 1981). The dereddened fluxes are given in Table 10. It is seen that the normalized dereddened fluxes do not depend very sensitively on the precise choice of the extinction curve.

The dereddened far-UV continuum is most likely due to stars in the exciting star cluster. The nebular emission in these wavelengths is negligible (Israel and Koorneef 1979). The contribution to the UV continuum from starlight reflected by dust particles remains a controversial matter (Lequeux *et al.* 1981). It depends not only on the amount of dust within the exciting cluster but also on the relative location of the dust particles and the ionizing stars. Because the latter information is unknown, we do not correct the UV continuum for scattered radiation but keep in mind that it may play an important role.

VI. DISCUSSION

We now assemble the observations in the different wavelength ranges together in an attempt to build a consistent physical picture for I Zw 36. We shall discuss in particular the dust and stellar content and the star formation history in I Zw 36. We also compare the properties of I Zw 36 with that of other extragalactic H II regions such as NGC 5471 and I Zw 18. The observed and dereddened continua for I Zw 36 from the optical to the far-UV are shown in Figure 10.

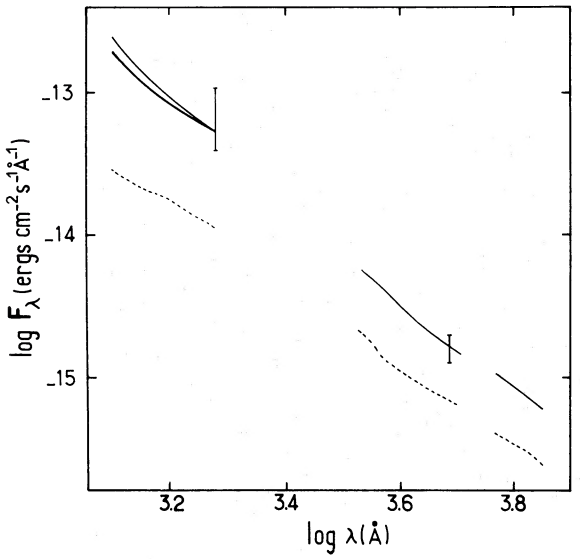

FIG. 10.—Continuum energy distribution of I Zw 36 from 1200 Å to 7400 Å. The dashed curve represents the observations. The solid curves represent the continuum emission after the reddening corrections discussed in §§ IV and V. The lower solid curve was obtained using the Galactic extinction law (Savage and Mathis 1979), and the upper solid curve was obtained using the extinction curve in the Small Magellanic Cloud (Rocca-Volmerange *et al.* 1981).

a) Dust Content

We would first like to determine the dust-to-gas mass ratio (in percent) in I Zw 36, which we shall denote by x_g. We use the optical data, because the optical extinction is produced by relatively larger dust grains than those responsible for the far-UV extinction and thus is more sensitively related to the dust content by mass. We consider in particular the extinction at the Hβ λ4861 line A_β. The extinction A_β is the sum of three terms:

$$A_\beta = A_{\beta\,\mathrm{Gal}} + A_{\beta\,\mathrm{ext}}(x_g) + A_{\beta\,\mathrm{int}}(x_g), \qquad (1)$$

where $A_{\beta\,\mathrm{Gal}}$ is the extinction from the Galaxy, $A_{\beta\,\mathrm{ext}}$ and $A_{\beta\,\mathrm{int}}$ are respectively the extinctions due to dust external and internal to the star formation region. We have assumed here that x_g is the same in both neutral and ionized gas components of I Zw 36.

The total extinction A_β can be determined in two ways. The first method uses the Balmer decrement. Using the galactic value for the ratio $A_\beta/E(\lambda - 4861)$ (§ IV), we derive $A_\beta(\mathrm{Balmer}) = 1.03 \pm 0.30$ mag. The second method uses the radio continuum flux associated with the line-emitting region (source 2 in § II*d*). With $T_e = 14{,}500$ K (§ IV), we find $A_\beta(\mathrm{radio}) = 0.89 \pm 0.25$ mag. These two quantities are directly comparable because the Hβ flux was measured through an aperture of 6″ diameter, larger than the 1.″6 FWHM size of the radio source. It is well known that for many extragalactic giant H II complexes, A_β(radio) is larger than A_β(Balmer). Maps of 30 Doradus in the Large Magellanic Cloud (Mills, Turtle, and Watkinson 1978), of NGC 595 (Viallefond, Donas, and Goss 1983), and NGC 604 (Viallefond 1983) where this is the case show clearly that this is due to dust mixed with ionized gas. For the case of I Zw 36, it is not clear that A_β(radio) is larger than A_β(Balmer) because of the uncertainties in the data. We will thus consider two cases: the first case where there is no internal dust, and the second case where there is both external and internal dust.

We first determine $A_{\beta\,\mathrm{Gal}}$, the extinction due to our Galaxy. Because of the high galactic latitude of I Zw 36 ($b^{\mathrm{II}} = 68°$), Galactic extinction is not very important. From the Galactic H I column density in the direction of I Zw 36 of 2×10^{20} H atoms cm^{-2}, and with $N(\mathrm{H\ I})/E(B-V) = 5.8 \times 10^{21}$ H atoms cm^{-2} mag^{-1} and $A_V/E(B-V) = 3.1$, we find $A_V = 0.11$ mag and $A_{\beta\,\mathrm{Gal}} = 0.13$ mag.

We consider now the case where all the dust is external to the line-emitting region and is associated with the H I in I Zw 36 itself. In this case $A_{\beta\,\mathrm{ext}} = 0.76 \pm 0.25$ mag. At the optical position of I Zw 36, 13″ from the centroid of the H I component 5 (§ II), the deconvolved H I column density is 2.0×10^{21} atoms cm^{-2} assuming a Gaussian distribution of the H I gas within component 5. The H I column density in front of I Zw 36 can also be derived using the damping wing of the absorption line at Lyman-α in the *IUE* spectrum (Fig. 9). Following the method given by Bohlin (1975), we determine $N(\mathrm{H\ I}) = 1.4 \times 10^{21}$ H atoms cm^{-2}. This means that about half the H I measured with the WSRT is in front of the ionized region. Using the equations given in Viallefond, Goss, and Allen (1982) and Viallefond (1983), we obtain a dust-to-gas mass ratio of $0.95 \pm 0.31\%$, similar to the solar neighborhood value of 0.7%. Given the fact that I Zw 36 has only a tenth of the solar metallicity, this is an unreasonably high dust-to-gas ratio.

We examine now the more realistic case where the extinction is both external and internal. In this case, equation (1) may be solved for x_g using either A_β (Balmer) with $A_{\beta\,\mathrm{int}}$(Balmer) or A_β(radio) with $A_{\beta\,\mathrm{int}}$(radio). The expressions for $A_{\beta\,\mathrm{int}}$(Balmer) and $A_{\beta\,\mathrm{int}}$(radio) can be found in the same papers quoted before. The two methods give consistent results. The first method gives $x_g = 0.30 \pm 0.13\%$ while the second method gives $x_g = 0.22 \pm 0.06\%$, where the uncertainties reflect the observational errors. Assuming that the dust-to-gas mass ratio is proportional to the metallicity, I Zw 36 is overabundant in dust by a factor of ~ 3 compared to the solar neighborhood. The dust-to-gas mass fraction x_g is also about 2 to 3 times larger than the value expected from the empirical relation between x_g and [O III]/Hβ for other extragalactic giant H II regions (Viallefond, Goss, and Allen 1982).

A possible solution to this problem is to have the extinction be mostly external but with the dust associated not with the H I gas but with molecular gas such as molecular hydrogen (Lequeux and Viallefond 1980). We may solve equation (1) for the column density of molecular gas required in front of the region of star formation (radio continuum source 2) to fit the observed extinction, assuming that the abundance of dust is proportional to the oxygen abundance ($x_g \sim 0.1\%$) as suggested by Viallefond, Goss, and Allen (1982). Using either A_β(Balmer) or A_β(radio), we derive $N(\mathrm{H\ I}+\mathrm{H_2}) \approx (7\pm3)\ N(\mathrm{H\ I})$. It is interesting to note that this amount of molecular gas is just what is needed to account for the virial mass derived in § II for H I component 5 and also for the whole galaxy ($M_V/M_\mathrm{H} \sim 5$). Moreover, a large amount of extinction due to dust associated with molecular gas would explain naturally the absence of bright optical emission at the position of the stronger radio continuum in I Zw 36 (source 1 in § II*d*).

If most of the mass of I Zw 36 is in molecular form, it is of interest to ask if CO emission at 115 GHz can be detected from the BCG. P. J. Encrenaz and R. W. Wilson have used the 7 m Bell Telephone Laboratories antenna (HPBW = 1'.7) to search for CO emission in the two BCGs I Zw 36 and I Zw 18 (private communication, 1982 November). CO was not detected in either galaxy at a level of ~ 0.01 K ($\sim 3\ \sigma$ per channel of 1 MHz).

It is interesting to discuss these results in terms of galactic giant molecular clouds (GMCs). Such clouds have an integrated temperature of $\sim 1.5\times10^4$ K pc^2 (Elmegreen, Elmegreen, and Morris 1980). At the distance of I Zw 36 (4.6 Mpc), the beam-smoothed brightness temperature of a single GMC would be ~ 0.004 K. Thus an upper limit of ~ 0.01 K would correspond to about three GMCs. With a typical mass of $10^5\ M_\odot$ of H_2 per GMC, the total H_2 mass in I Zw 36 is less than $3\times10^5\ M_\odot$, a factor of 500 smaller than the virial mass of component 5 alone. It is clear that, if molecular hydrogen were to account for the virial mass, the value of the CO/H_2 abundance ratio in I Zw 36 has to be much smaller than the galactic value. This is not implausible since there are several factors which may cause CO to be deficient relative to H_2 in BCGs (Elmegreen, Elmegreen, and Morris 1980): (*a*) decreased C and O abundances relative to H (we have shown that I Zw 36 is deficient by a factor of ~ 10 in O [§ IV] and $\gtrsim 10$ in C [§ VI*b*] compared to the solar neighborhood), (*b*) decreased dust-to-gas abundance ratios (x_g). We have shown in § VI*a* that, if 90% of the gas is H_2, x_g in I Zw 36 is $\sim 0.1\%$, only a tenth of the solar value.

b) Star Formation

We now use our observations to try to answer the following questions:

1. What are the properties of the present burst of star formation; i.e., what is the initial mass function (IMF), the star formation rate (SFR), and the age or duration of the burst?

2. Has there been previous star formation in I Zw 36? Is the present burst the first one in its history? If not, how many burst were there previously to the present one?

Our approach is the following. We describe the present star formation by four parameters. The first parameter is the slope x of the IMF defined such that $dn(M)/d\ln M \propto M^{-x}$. The second and third parameters are m_L and m_U, respectively the lower and upper stellar mass cutoffs of the IMF. The fourth parameter is a time parameter called τ. We consider two limiting models of star formation. The first one is the case of an infinitely short burst (ISB). In this case τ is the age of the burst. The second one is the case of continuous star formation (CSF) where stars are formed continuously with a constant SFR until now. In this case τ is the duration of the burst. The methods for constructing these models are similar to those described by Lequeux *et al.* (1981). The evolution of a star cluster on the main sequence is computed using evolutionary tracks (Iben 1967; Chiosi, Nasi, and Sreenivasan 1978) and stellar atmospheres models (Kurucz 1979).

Our models are then used to calculate the following five quantities which are used as observational constraints:

1. $W(\mathrm{H}\beta)$, *the equivalent width of the* Hβ λ4861 *line.* This quantity is relatively insensitive to reddening corrections, but is very sensitive to all parameters except m_L if $m_L \ll 2\ M_\odot$. It gives information on the number of A and B stars which dominate the continuum at Hβ relative to the number of O stars which provide the ionization responsible for the Hβ line. $W(\mathrm{H}\beta)$ is calculated by:

$$W(\mathrm{H}\beta)(\text{Å}) = 4.785\times10^{-13} N_\mathrm{Lyc}/I_{4862,\mathrm{cont}},$$

where N_Lyc is the number of Lyman continuum photons in photons s^{-1} and $I_{4862,\mathrm{cont}}$ is the continuum flux density at 4862 Å in ergs s^{-1} Å^{-1}. This quantity decreases rapidly to zero after $\sim 5\times10^6$ years in the ISB model, but the decrease is much slower in the CSF model (Fig. 11).

2. T_eff, *the effective temperature*, defined as the effective temperature of a star producing the same ratio of hydrogen Lyman continuum photons emitted above and below the helium Lyman limit at 504 Å (Lequeux *et al.* 1981). This quantity depends strongly on x and m_U. It decreases rapidly with time in the ISB model but reaches as asymptotic value after about 5 million years in the CSF model (Fig. 12).

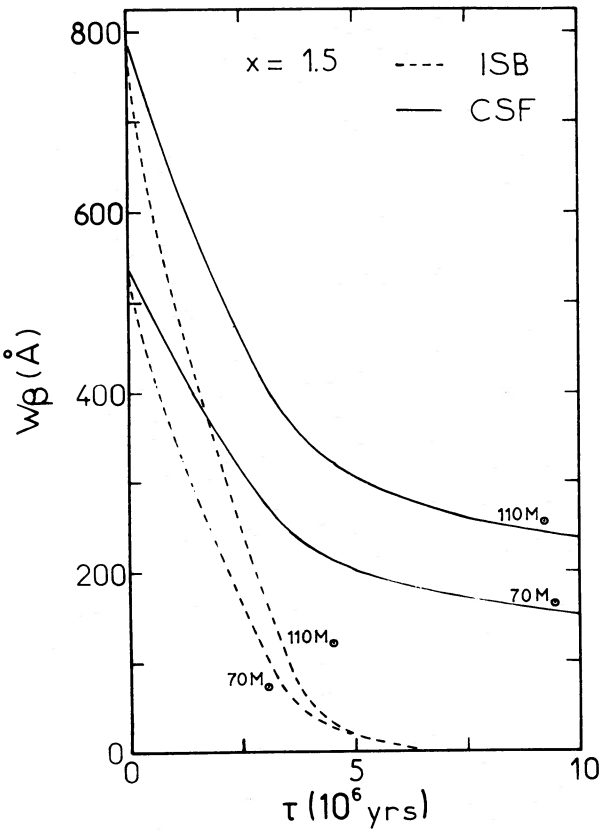

FIG. 11

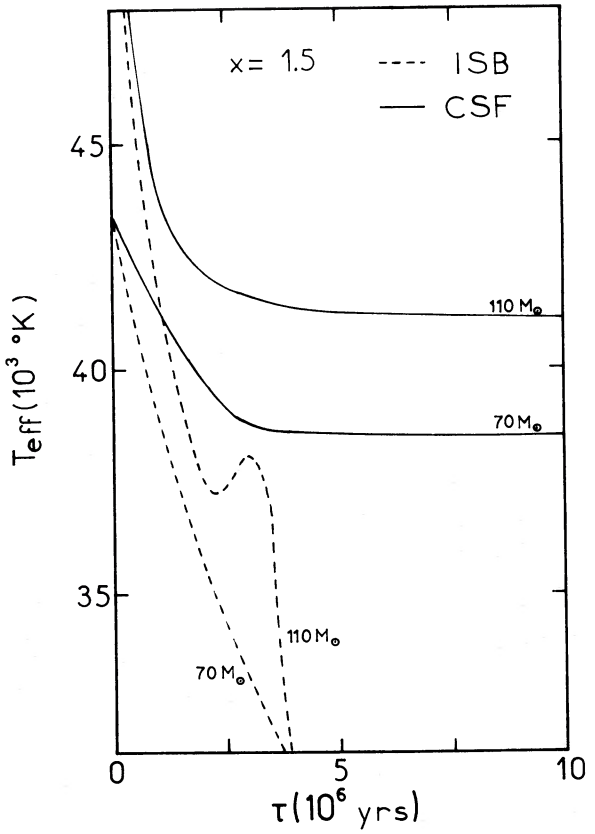

FIG. 12

FIG. 11.—Equivalent width W_β for a young star cluster of the Hβ Balmer line as a function of the age τ of an infinitely short burst (ISB) or the duration τ of an ongoing burst of continuous star formation (CSF). These curves are computed for a slope $x = 1.5$ of the initial mass function (IMF) and for stars with masses between 1.8 $M_\odot$ and 70 or 110 $M_\odot$. In the ISB model, W_β reaches zero after $\sim 5\times10^6$ years because of the death of the massive stars. In the CSF model, W_β decreases rapidly for $\tau \lesssim 4\times10^6$ years because of a rapid decrease of the Lyman continuum luminosity but decreases more slowly afterwards. This is because the Lyman continuum flux becomes roughly constant with time but the continuum emission at 4861 Å continues to increase slowly.

FIG. 12.—Effective temperature $T_{\rm eff}$ as a function of τ for the same models as in Fig. 11. In the CSF model $T_{\rm eff}$ remains constant for $\tau \gtrsim 5\times10^6$ years because the Lyman continuum luminosity reaches a steady state. The bump in the dashed curve is caused by the rapid variation of $T_{\rm eff}$ for the most massive stars before they leave the main sequence, causing a rapid decrease of $T_{\rm eff}$.

3, 4 and 5. *The spectral indices* $\alpha(4087,4462)$, $\alpha(4462,4812)$, *and* $\alpha(1608,4862)$, defined as:

$$\alpha(\lambda_1,\lambda_2) = \left| \frac{\log\left[I_{\lambda_1\,\rm cont}/I_{\lambda_2\,\rm cont}\right]}{\log(\lambda_1/\lambda_2)} \right|.$$

These quantities permit one to constrain the models in reproducing the observed stellar continuum. The first two spectral indices characterize the optical continuum where the reddening corrections are secure. They depend more sensitively on x and m_L (for $m_L > 2\ M_\odot$) than on m_U, the continuum in the 4000 Å to 5000 Å region being provided mainly by B2–B9 and early A main-sequence stars. The last spectral index links the UV and optical regions. It can, in principle, give informations on stellar masses in the 8–10 $M_\odot$ ranges, i.e., on B0 to B3 main-sequence stars. It is less well determined observationally than the other spectral indices because it makes use of the UV continuum which has a large extinction correction and may be contaminated by scattered light (§ V). We shall only use the last quantity as an additional check but not as a model constraint, since the first four observational constraints are sufficient to determine uniquely our four-parameter star formation model.

We list in Table 11 the observational constraints for I Zw 36, along with that for another very metal-deficient BCG ($Z \sim Z_\odot/30$), I Zw 18, and for a H II complex in M101, NGC 5471 ($Z \sim Z_\odot/3$), for comparison. The

TABLE 11

OBSERVATIONAL PROPERTIES OF THE STAR CLUSTERS IN THE TWO BCGS I Zw 36 AND I Zw 18 AND THE M101 COMPLEX NGC 5471

Parameter	I Zw 36	NGC 5471	I Zw 18
$W(\mathrm{H}\beta)$ (Å)	238 ± 23	185 ± 15[a]	100 ± 7[a]
T_{eff} (10^4 K).....	4.2 to 5.0	4.0 to 4.6[b]	4.0 to 5.5[c]
$\alpha_{4087-4462}$	-3.85 ± 0.39	-3.09[a]	$-3.3^{+0.2}_{-0.4}$[a]
$\alpha_{4462-4812}$	-3.56 ± 0.04	-3.06[a]	$-3.6^{+0.3}_{-1.0}$[a]
$\alpha_{1608-4862}$	-3.58 ± 0.25	-4.64 ± 1.32[a]	-5.04 ± 1.20[a]

SOURCE.—[a]Sargent and Searle 1970 and *IUE* archives. [b]Rayo, Peimbert and Torres-Peimbert 1982. [c]Lequeux *et al.* 1979.

error bars in the spectral indices reflect the uncertainties in the reddening corrections.

We first discuss the CSF model for I Zw 36. We find that the best model is characterized by $x \sim 1.5$, $m_U \sim 100\ M_\odot$, $m_L \sim 4\ M_\odot$, and $\tau \sim 7 \times 10^6$ years. The star formation rate in this best model is $0.007 \pm 0.001\ M_\odot\ \mathrm{yr}^{-1}$. The IMF slope $x = 1.5$ is close to the Salpeter solar neighborhood value of 1.35, but significantly flatter than the more recent value of 2 obtained by Lequeux (1979) for stellar masses greater than $1.8\ M_\odot$. If the IMF given by Lequeux (1979) ($x = 0.6$ for $m < 1.8\ M_\odot$ and $x = 2$ for $m > 1.8\ M_\odot$) is used, the model produces too flat an optical continuum in the sense of a flux deficiency in the blue, independently of m_U and τ. The IMF has to be truncated at the lower mass end at $\sim 4\ M_\odot$ because the model cannot fit simultaneously $W(\mathrm{H}\beta)$ and the other parameters. For example, with $x = 1.5$, $m_U = 110\ M_\odot$, $m_L = 0.007\ M_\odot$, and $\tau = 3 \times 10^6$ years, the model gives $\alpha(4087,4462) = 3.47$, $\alpha(4462,4812) = 3.51$, and $T_e = 41{,}600$ K, in good agreement with the observational values (Table 11). However, the predicted value of $W(\mathrm{H}\beta)$ is 407 Å, which is significantly larger than the observed value of 238 ± 23 Å. Increasing τ would reduce $W(\mathrm{H}\beta)$ but would simultaneously increase the optical indices.

The ISB model can reproduce the observational constraints with $x \sim 1.5$ for $m > 1.8\ M_\odot$ and $x \sim 0.6$ for $m < 1.8\ M_\odot$, $m_U \sim 120\ M_\odot$, $m_L \lesssim 4\ M_\odot$, and $\tau \sim 3 \times 10^6$ years. The total mass of the stars formed is $(1.4 \pm 0.3) \times 10^5\ M_\odot$ for $m_L = 0.007\ M_\odot$. The difficulties with steeper IMF for $m > 1.8\ M_\odot$ are the same as in the CSF model: the predicted optical continuum is too flat compared to what is observed.

Both the CSF and ISB models give a value of $\alpha(1608-4862)$ of ~ 3.1, smaller than the value given in Table 11. The models do not produce enough UV fluxes relative to the optical fluxes. This discrepancy may be explained by a smaller value for the C/O ratio by a factor varying from 1.2 to 2.2 as compared to the solar neighborhood and/or a significant contribution to the UV continuum from stellar light scattered by dust. Dufour, Shields, and Talbot (1982) have found that the C/O ratio is smaller relative to the Sun in metal-deficient galaxies. Bohlin (1982) has found that the UV flux from the Orion nebulosity is about 2.5 times the stellar UV fluxes from the Trapezium stars, suggesting an important contribution from scattered light.

It is now interesting to compare I Zw 36 with the BCG I Zw 18 and the M101 H II complex NGC 5471. The best CSF model for I Zw 18 is characterized by $x = 1.5$, $m_U \sim 100\ M_\odot$, $m_L \lesssim 2\ M_\odot$, and $\tau \sim 3 \times 10^7$ years. As in the case of I Zw 36, the IMF slope for $M > 1.8\ M_\odot$ in I Zw 18 is significantly flatter than Lequeux's (1979) slope. The lower mass cutoff is smaller and the burst age is larger in I Zw 18 essentially because $W(\mathrm{H}\beta)$ is much smaller in I Zw 18 than in I Zw 36 for similar effective temperatures. The model predicts smaller UV fluxes than the dereddened observed fluxes. However, the extinction corrections in the UV are unknown in the case of I Zw 18. The value of $\alpha(1608,4862)$ listed in Table 11 has been derived by assuming quite arbitrarily that $A_{1900}/E(B-V) = 12.2$ as in the case of the Small Magellanic Cloud (Rocca-Volmerange *et al.* 1981).

The best CSF model for NGC 5471 is characterized by the solar neighborhood IMF given by Lequeux (1979), $m_U \sim 110\ M_\odot$, $m_L \sim 0.007\ M_\odot$, and $\tau \sim 5 \times 10^6$ years. However, the model gives $\alpha(1608,4862) = 2.93$, significantly smaller than the value given in Table 11. The model predicts insufficient UV flux relative to the optical flux. The excess of observed UV flux may be due to a significant contribution of scattered stellar light by dust and/or to a deficiency of C relative to O as compared to the solar neighborhood. In the latter situation, the UV extinction would have been overestimated. It is interesting to note that if the slopes of the IMF in the three objects are compared, there appears to be a tendency for flatter IMF in metal-deficient BCGs as compared with more metal-rich H II complexes in late-type galaxies.

After discussing the properties of the present starburst in I Zw 36, we now use the observed metallicity to put constraints on possible previous massive star formation.

We use the results of Lequeux *et al.* (1981) for the oxygen production. In the case of the ISB model which gives $\tau \sim 3 \times 10^6$ years, the massive stars have not had sufficient time to evolve and manufacture the observed amount of metals. Hence there must have been massive star formation in the past. If these stars were made in bursts of strength comparable to the present one, one previous burst is sufficient to manufacture $\sim 1820\ M_\odot$ of oxygen, which is comparable to the total oxygen mass of $1900 \pm 300\ M_\odot$ deduced in § IV, assuming that the metallicity of the H II region is characteristic of the entire H I component 5. This last assumption is reasonable since the diffusion time of metals from the ionized region into the entire neutral region is $\sim 4 \times 10^7$ years, much shorter than the time interval between bursts. In the CSF model, $228 \pm 50\ M_\odot$ of oxygen have been made in the last 7×10^6 years. During that time, the metals could have diffused over a distance of ~ 70 pc, larger than the H II region diameter of 59 pc (Table 4). Since the observed oxygen mass associated with the H II region is only $16 \pm 3\ M_\odot$ (§ IV), more than 90% of the oxygen produced must have diffused into the H I gas. There is no need for previous massive star formation in this case.

c) *Old Stellar Population*

The UV and optical data discussed before give information on high ($M > 30\ M_\odot$) and intermediate ($M \gtrsim 2\ M_\odot$) mass stars. To obtain information on lower mass stars, near-infrared observations (§ III) are needed. The $J - K$ color of the stellar continuum, after corrections for extinction and ionized gas emission (Table 5), is ~ 0.45. To compare with the stellar data of Johnson (1966) which is characterized by solar metallicity, we need to correct for metallicity effects since Z(I Zw 36) $\sim Z_\odot/10$. Increasing the metallicity by a factor 10 corresponds to a reddening in $J - K$ of ~ 0.14 mag (Thuan 1983). Thus the $J - K$ color for I Zw 36 corrected for metallicity is ~ 0.59 mag. The mean spectral type for giant stars corresponding to this color is G8. We feel that the observed near-infrared fluxes come from giant but *not* from supergiant stars for the following reasons: (1) The near-infrared observations were obtained at a position where there is no strong optical emission; thus the presence of supergiant stars there is very unlikely. (2) The $(J - K)$–metallicity relationship for BCGs is the same as that for globular clusters whose light, we know, is dominated by giant stars (Thuan 1983).

There is, then, an old stellar population of G and K giants in I Zw 36 with an age larger than a few billion years. This conclusion is not specific to I Zw 36 but is true for all BCGs observed in the near-infrared (Thuan 1983). These stars must have been made previously to the present burst. The time scales derived earlier ($\tau \sim 3 \times 10^6$ years in the ISB model and $\tau \sim 7 \times 10^6$ years in the CSF model) are not long enough for stars made in the present burst to evolve to the giant stage. In the ISB model, these giants have evolved from stars of a few solar masses made in the previous burst. In the CSF model, the formation of high- and intermediate-mass stars and that of low-mass stars appear to be uncoupled. In the present burst, we have seen that the IMF needs to be truncated at $\sim 4\ M_\odot$ to fit the observations. In the past, in order to account for the giant population and not to violate the metallicity constraint, only low-mass star formation could have occurred. In the CSF model, a continuous rate of low-mass star formation would also help to understand why the hydrogen clouds composing I Zw 36 have not gravitationally collapsed until recently. The most massive H I cloud in I Zw 36 (component 5, § II) has a Jeans collapse time scale of only $\sim 10^8$ years in the absence of rotation, much shorter than the galaxy lifetime. Low-mass star formation can inject heat into the H I clouds to prevent their gravitational collapse (Silk 1980).

Can the old stellar population of G and K giants account for the virial mass derived in § II*b* from H I interferometric observations? To answer this question, we use the models constructed by Struck-Marcell and Tinsley (1978) in the $(U - B, V - K)$-plane. We combine our infrared measurements with Huchra's (1977) *UBV* measurements to derive $U - B = -0.63 \pm 0.04$ and $V - K = 0.44 \pm 0.12$ within an 8″ aperture. This procedure is, of course, only valid if the old stellar population underlies the region of star formation. These colors are used in conjunction with the models to derive a ratio of the mass of stars made during the present burst to the mass of stars made previously approximately equal to unity. In the ISB model, the mass of stars made in the present burst is $(1.4 \pm 0.3) \times 10^5\ M_\odot$ for $m_L = 0.007\ M_\odot$. In the CSF model, the mass of stars made in the present burst up to now is $(5.0 \pm 1.0) \times 10^4\ M_\odot$. Since the masses in old and young stars are comparable, the old stellar population fails by more than three orders of magnitude to account for the virial mass ($\sim 2 \times 10^8\ M_\odot$) if it is coextensive spatially with the young stellar population. If the old stellar population were to constitute the virial mass in I Zw 36, it has to be spatially much more extended than the young stellar population in the present burst. Only then would the integrated $V - K$ become redder than the value observed through the 8″ aperture and the mass of the old stellar population become larger. In this case, low-mass continuous star formation without massive star formation needs to be invoked even in the ISB model, since at most $1.4 \times 10^5\ M_\odot$ of stars will have been made in the past burst. Of course, there would be no need for the old stellar population to be spatially more extended than the young stellar population if the virial mass is made up of another constituent, such as molecular hydrogen (§ VI*a*).

In summary, the optical observations of I Zw 36 can be fitted equally well by both ISB and CSF models. Both require an IMF with a slope of 1.5, close to the Salpeter value of 1.35, and a burst age or duration of a few million years. The CSF model requires a cutoff at the low mass end of the IMF at $\sim 4\ M_\odot$. To reproduce the observed metallicity, there must have been one previous burst of comparable strength to the present burst in the ISB model, while *no* previous massive star formation is needed in the CSF model. The near-infrared observations indicate the presence of an old stellar population of G and K giants. These giants may have evolved from stars made in a previous burst of star formation in the ISB model, or in a continuous low-mass star formation process in the CSF model. The old stellar population cannot account for the virial mass derived by the H I interferometric observations if the young and old populations are coextensive spatially. In that case, the virial mass must be made up of something else than old stars. Molecular hydrogen appears to be a good candidate.

VII. SUMMARY

We present in this paper radio, near-infrared, optical, and ultraviolet observations of the blue compact dwarf galaxy (BCG) I Zw 36 ≡ Mrk 209 ≡ Haro 29. The main observational results follow:

1. The H I distribution shows a core-halo structure. The core contains about half of the total H I mass. The halo is diffuse and contains several H I clumps.

2. The visible star formation region is associated with the H I core. Its position is slightly shifted with respect to the H I peak density.

3. There are not uniquely turbulent motions. There is a systematic velocity gradient associated with the H I core.

4. The virial mass of the BCG is 5 to 7 times the H I mass.

The four above properties appear to be common to all BCG which have been observed with an H I interferometer.

5. There are two radio continuum sources associated with the H II complex in I Zw 36. One is associated with the brightest optical knot and has a flux density of 1.25 ± 0.24 mJy at 5 GHz. The other has a flux density of 3.4 ± 0.03 mJy and a flat spectrum between 1.4 and 5 GHz. It does not have strong optical emission associated with it, probably because of the large dust extinction there (see result 8).

6. The near-infrared observations indicate the presence of an old stellar population of G and K giants.

7. Like all other BCGs, I Zw 36 is metal-deficient with respect to the Sun: $Z \sim Z_\odot/10$.

8. The dust-to-oxygen abundance ratio by mass is ~ 3 times greater in I Zw 36 than in the solar neighborhood. This large amount of dust can be explained if it is associated with invisible molecular hydrogen gas with mass equal to the virial mass, assuming that the dust abundance is proportional to the metallicity.

We have used these observations to study star formation in I Zw 36 in the context of two limiting models: the infinitely short burst (ISB) model and the continuous star formation (CSF) model. We cannot distinguish between the ISB and CSF models. The optical spectrophotometric observations can be fitted equally well by both models. Both models require an IMF with a slope of 1.5 close to the Salpeter value of 1.35 and a burst age or duration of a few million years. The CSF model requires a cutoff at the low-mass end of the IMF at $\sim 4\ M_\odot$. No previous massive star formation is needed in the CSF model, but the ISB model requires one previous burst to account for the observed metallicity. The giant old stellar population can be made in the previous burst in the ISB model or in previous continuous low-mass star formation in the CSF model.

The nature of the main constituent of the total mass remains an open problem. The old stellar population can account for the virial mass (result 4) only if it is much more extended spatially than the young population. In that case, low-mass stars must have formed in the past independently from the burst producing the massive stars. The possibility that molecular hydrogen provides a substantial part of the total mass cannot be excluded. Very indirect evidence based on the dust content in I Zw 36 suggests that the molecular hydrogen column density is 6 ± 3 times that of neutral hydrogen, about the quantity needed to account for the virial mass. BCGs may be significantly more gas-rich than previously believed.

This multifrequency study was made possible because of the generous amounts of observing time granted at the many observatories cited in the text. We are grateful to the staffs at these observatories for their helpful assistance.

The Westerbork Radio Observatory is operated by the Netherlands Foundation for Radioastronomy with the financial support of the Netherlands Organization for the Advancement of Pure Research.

F. V. is grateful to the University of Groningen for their hospitality and for the use of their Computing Center.

T. X. T. thanks the Astrophysics group at Saclay for their warm hospitality and acknowledges financial support from the Research Corporation, NASA, the French Commissariat à l'Energie Atomique and a Sesquicentennial Associateship Award from the Center for Advanced Studies of the University of Virginia.

We thank Dr. James Lequeux for useful comments, and Drs. Pierre Encrenaz and Robert Wilson for communicating their CO measurements.

REFERENCES

Balkowski, C., Chamaraux, P., and Weliachew, L. 1978, *Astr. Ap.*, **69**, 263.
Bohlin, R. 1975, *Ap. J.*, **200**, 402.
_____. 1982, preprint.
Brocklehurst, M. 1971, *M.N.R.A.S.*, **153**, 471.
Burbidge, E. M., and Burbidge, G. R. 1975, in *Galaxies and the Universe*, ed. A. Sandage, M. Sandage, and J. Kristian (Chicago: University of Chicago Press), p. 81.
Cassé, J. L., and Müller, C. A. 1974, *Astr. Ap.*, **31**, 333.
Chiosi, C., Nasi, E., and Sreenivasan, S. R. 1978, *Astr. Ap.*, **63**, 103.
Dufour, R. J., Shields, G. A., and Talbot, R. J. 1982, *Ap. J.*, **252**, 461.
Elmegreen, B. G., Elmegreen, D. M., and Morris, M. 1980, *Ap. J.*, **240**, 455.
French, H. B. 1980, *Ap. J.*, **240**, 41.
Gottesman, S. T., and Weliachew, L. 1972, *Ap. Letters*, **12**, 63.
Heiles, C. 1975, *Astr. Ap. Suppl.*, **20**, 37.
Huchra, J. P. 1977, *Ap. J. Suppl.*, **35**, 171.
Iben, I., Jr. 1967, *Ann. Rev. Astr. Ap.*, **5**, 571.
Israel, F. P., Goss, W. M., and Allen, R. J. 1975, *Astr. Ap.*, **40**, 421.
Israel, F. P., and Koorneef, J. 1979, *Ap. J.*, **230**, 390.
Johnson, H. L. 1966, *Ann. Rev. Astr. Ap.*, **4**, 193.
Kennicutt, R., Balick, B., and Heckman, T. 1980, *Pub. A.S.P.*, **92**, 134.
Kinman, T. D., and Davidson, K. 1981, *Ap. J.*, **243**, 127.
Kunth, D. 1981, Thèse d'Etat, Université Paris VII, France.
Kurucz, R. L. 1979, *Ap. J. Suppl.*, **40**, 1.
Lequeux, J. 1979, *Astr. Ap.*, **80**, 35.
Lequeux, J., Maucherat-Joubert, M., Deharveng, J. M., and Kunth, D. 1981, *Astr. Ap.*, **103**, 305.
Lequeux, J., Peimbert, M., Rayo, J. F., Serrano, A., and Torres-Peimbert, S. 1979, *Astr. Ap.*, **80**, 155.
Lequeux, J., and Viallefond, F. 1980, *Astr. Ap.*, **91**, 269.
Mills, B. Y., Turtle, A. J., and Watkinson, A. 1978, *M.N.R.A.S.*, **185**, 263.
Nandy, K., Morgan, D. H., Willis, A. J., Wilson, R., Gondhalekar, P. M., and Houziaux, L. 1980, *Nature*, **283**, 725.
Oke, J. B. 1974, *Ap. J. Suppl.*, **27**, 21.
Rayo, J. F., Peimbert, M., and Torres-Peimbert, S. 1982, *Ap. J.*, **255**, 1.
Rocca-Volmerange, B., Prevot, L., Ferlet, R., Lequeux, J., and Prevot-Burnichon, M. L. 1981, *Astr. Ap.*, **99**, L5.
Rosa, M. 1980, *Astr. Ap.*, **85**, L21.
Sargent, W. L. W., and Searle, L. 1970, *Ap. J.* (*Letters*), **162**, L155.
Savage, B. D., and Mathis, J. S. 1979, *Ann. Rev. Astr. Ap.*, **17**, 73.
Shields, G. A., and Searle, L. 1978, *Ap. J.*, **222**, 821.
Silk, J. 1980, in *Star Formation* (Saas-Fee: Geneva Observatory), p. 166.
Struck-Marcell, C., and Tinsley, B. M. 1978, *Ap. J.*, **221**, 562.
Stasinska, G. 1982, *Astr. Ap. Suppl.*, **48**, 299.
Stone, R. P. S. 1974, *Ap. J.*, **193**, 135.
Thuan, T. X. 1983, *Ap. J.*, **268**, in press.
Thuan, T. X., Fanelli, M., and O'Connell, R. W. 1983, in preparation.
Thuan, T. X., and Martin, G. E. 1981, *Ap. J.*, **247**, 823.
Viallefond, F. 1983, in preparation.
Viallefond, F., Donas, J., and Goss, W. M. 1983, *Astr. Ap.*, in press.
Viallefond, F., Goss, W. M., and Allen R. J. 1982, *Astr. Ap.*, 115, 373.
Whitford, A. E. 1958, *A. J.*, **63**, 201.
Zwicky, F. 1971, *Catalogue of Selected Compact Galaxies and of Post Eruptive Galaxies* (Bern, Switzerland).

TRINH X. THUAN: Astronomy Department, University of Virginia, P.O. Box 3818, University Station, Charlottesville, VA 22903

FRANCOIS VIALLEFOND: Observatoire de Paris, Meudon, F-92190 Meudon, France